DEPARTAMENT D'ASTRONOMIA I METEOROLOGIA

UNIVERSITAT DE BARCELONA

Near-relativistic electron events. Monte Carlo simulations of solar injection and interplanetary transport

Memòria presentada per
Neus Àgueda Costafreda
per optar al grau de Doctora
per la Universitat de Barcelona.
Barcelona, 20 de febrer de 2008

6 Study of solar near-relativistic electron events. II

In this chapter we apply the deconvolution procedure to the study of five of the electron events selected in Chapter 5, which show long rise phases (longer than one hour). We analyze each NR electron event from the point of view of the observations (the electromagnetic proxy emissions and the characteristics of in-situ SEPs observed at 1 AU). Then, we present the results of the application of the deconvolution algorithm. The events are analyzed in order of increasing Δ: Sep04, Dec01, May98, Jul00 and Apr01.

6.1 The 2004 September 19 event

6.1.1 Electromagnetic emissions

An M1.9 soft X-ray flare (onset at 16:46 UT and maximum at 17:12 UT) was observed by *GOES* in association with the NR electron event observed by the *ACE* spacecraft on 2004 September 19. No Hα flare was reported by the *SGD*. However, Cane et al. (2006) estimated the flare site at N03W58 based on the locations of the active regions. *RHESSI* observed hard X-ray emission at 25–50 keV starting at 16:48 UT and lasting ~15 min.

A CME structure was seen by LASCO C3 coronagraph at 22:42 UT, when it was already at 31 $R_\odot$. The CME feature was not reported when it was closer to the Sun because measurements from the C2 coronagraph were unavailable. Cane et al. (2006) reported the passage of an interplanetary shock at *ACE* around 06:00 UT on 2004 September 22 with associated transit speed of 690 km s^{-1} (shock transit time from the Sun to 1 AU of 60 h)[1].

Type III bursts were observed from 16:55 UT to 17:30 UT by *Wind*/WAVES. A possible very sporadic 14–2.5 MHz type II burst was also reported from 17:15 UT to 18:15 UT by the *Wind*/WAVES experiment .

[1] Cane et al. (2006) listed the shock transit time but not its transit speed.

6.1.2 In-situ energetic particles

Figure 6.1 shows the spin-averaged 62–312 keV electron intensities observed by the EPAM-/LEFS60 telescope from September 19 (DOY 263) to September 23 (DOY 267). The first NR electrons were detected above the pre-event background at 17:19 UT in the E'4 channel. The maximum spin-averaged intensity was observed at 18:44 UT in the E'4 channel, at 19:12 UT in the E'3 channel and at 20:04 UT in the E'2 channel. We will study this event for the period from 17:19 UT to 20:45 UT (gray area in Figure 6.1). For comparison, the top panel in Figure 6.1 shows the DE30 electron intensities (thin line). The similar trends indicate that there is negligible ion contamination in the LEFS60 NR electron profiles during the selected time period, but not during most part of DOY 264 and 265.

The first panel in Figure 6.1 also includes the 8-min proton intensities observed by the LEMS120 and the ERNE telescope (thin line) between 1 and 5 MeV approximately. Although these two telescopes are not cross-calibrated, we are able to compare their measurements if we assume that both telescopes measure the same values of pre-event intensity background, when the profiles are almost flat and isotropic[2]. The beginning of the proton event was first observed by *ACE* at 18:00 UT. Unfortunately, there are gaps in the proton data from ERNE and it is not possible to estimate the onset of the event and compare it with the onset of the event at *ACE*.

The P'7 proton intensity profile shows an increase of two orders of magnitude in the 18 h following the onset. Then the intensities remain nearly constant for ∼14 h, until 265/06:00 UT, and finally decay to the background level in the following ∼42 h. After 264/11:00 UT, NR electron profiles measured by LEFS60 track the proton profiles. Deflected electron intensities do not show this behavior, which is a clear indication that the LEFS60 channels are contaminated by energetic protons after this time.

Cane et al. (2006) studied the event-averaged abundance of Fe relative to O at energies above 25 MeV nucl^{-1}, from 263/17:12 UT to 264/17:12 UT, using the *ACE*/SIS instrument and reported a ratio of Fe/O = 1.6 ± 1.1. Therefore, they concluded that this SEP event could include particles accelerated in the flaring processes[3]. Note that the reported Fe/O value was associated with high uncertainties.

The four lower panels in Figure 6.1 show the solar wind velocity and the three components

[2]In Figure 6.1, the ERNE low energy channel (1.33–1.90 MeV) is multiplied by a factor 5, whereas the high energy channel (1.90–4.75 MeV) is multiplied by 0.1.

[3]Cane et al. (2006) reported Fe to O abundance ratios normalized to the average value derived by Reames (1998) for 49 large SEP events in the energy range 5–12 MeV nucl^{-1} (Fe/O = 0.134). Cane et al. (2006) assumed that normalized Fe/O ratios higher than 2 indicate events with an average composition that includes a significant contribution from flare particles, whereas normalized Fe/O ratios lower than 1 indicate events with an average composition that is below the typical coronal value.

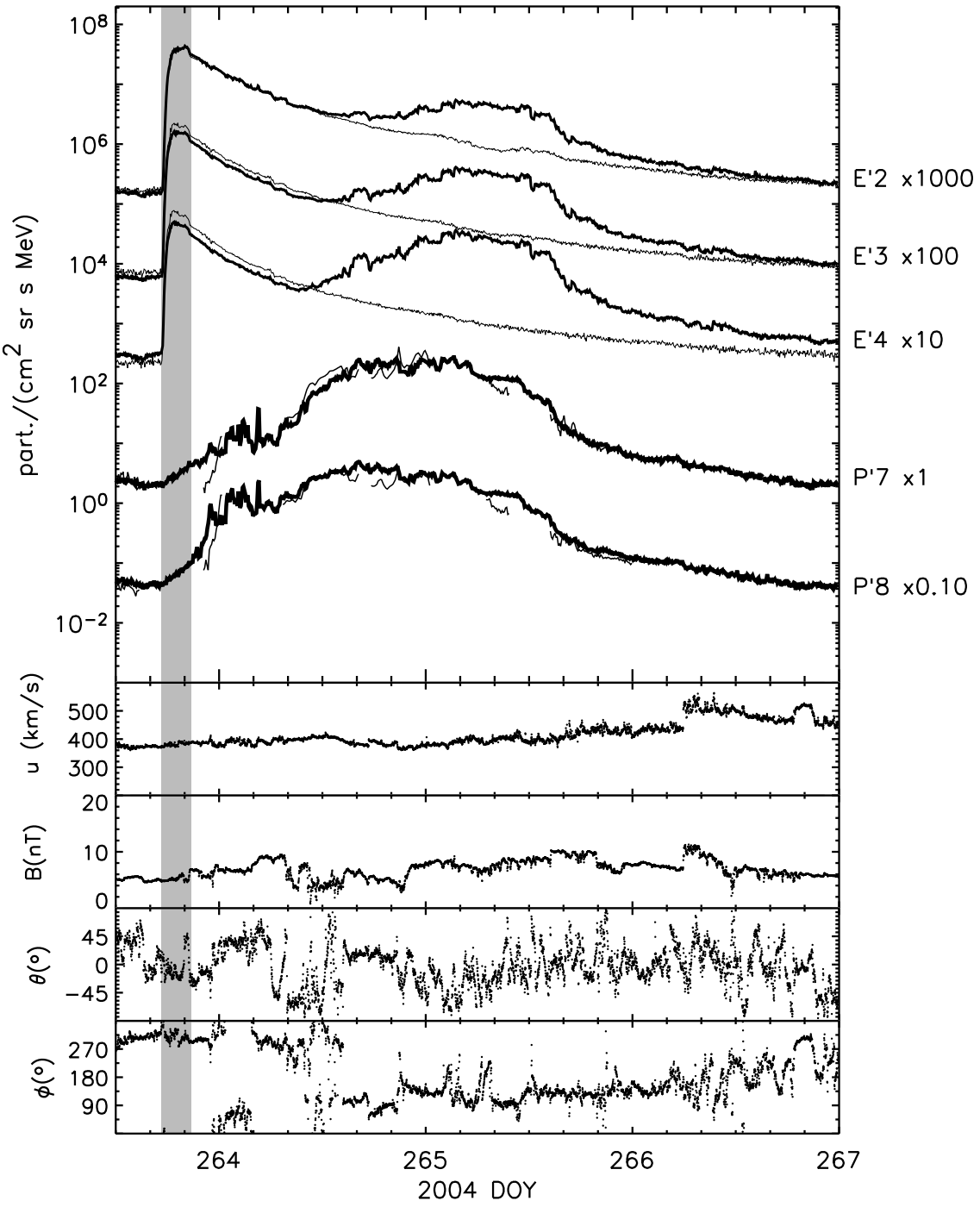

Figure 6.1: Sep04 event: Particle event, solar wind and magnetic field components in the RTN coordinate system. Same presentation as in Figure 5.1.

of the IMF in the RTN spacecraft coordinate system. SWEPAM data indicate that at the beginning of the event, *ACE* was embedded in a solar wind stream with a mean velocity of 376 km s^{-1}. Both the solar wind velocity and the IMF direction were stable through the period studied. The nominal footpoint of the field line connecting *ACE* to the Sun was at W64, as estimated from the observed solar wind speed, quite close to the longitude of the flare site (W58). The spectral index of the derived differential intensity spectrum is estimated by $\gamma = 2.1$. Therefore, we assume $\gamma_s = 2.6$ as a first approximation of the spectral index of the source (see section 3.6).

6.1.3 Deconvolution of the NR electron event

Figure 6.2 shows the *ACE*/MAG magnetic field measurements in the spacecraft coordinate system, the range of μ-values scanned by the LEFS60 telescope and the μ-co of the telescope for the period under study. As can be seen, the IMF polarity remains positive during the period under study; this means that electrons coming from the Sun along the field lines have $\mu = 1$. The μ-co of the telescope varies between 40% and 100%, with a mean coverage of ~88%. As the telescope scans particles propagating antisunward along the field direction (gray area in panel four) and μ-co $\geq$ 70%, , sectored data provides a detailed description of the NR electron event.

Note that for a 10 min period around 17:35 UT, during the rising phase of the event, the μ-co decreases to ~40%[4]. After 17:40 UT, the μ-co of the telescope is of 90% and it remains higher than 80% until the end of the selected time period. Note also that from 18:30 UT to 19:50 UT, $\phi_B \simeq 0^\circ$ and pairs of sectors scan the same range in pitch-angle cosine; i.e. the mean pitch-angle cosine scanned by them is very similar (see fourth panel in Figure 6.2).

We simulate this electron event following the procedure described in section 5.2.3 for the May00 event. The lowest values of ζ obtained for each scattering case are listed in Table 6.1. Figure 6.3 shows the fit for the case with the lowest ζ; it corresponds to $\lambda_r = 0.20$ AU and isotropic scattering. The fit succeeds in reproducing most of the profiles during more than three hours.

The values of the solar electron injection derived from the best fit are shown in the three top panels of Figure 6.4. The injection profile clearly shows one single component starting around 17:00 UT and extending in time for at least three hours. Injection starts at 17:05 UT in E'2, at 17:09 UT in E'3 and at 17:11 UT in the E'4 energy channel.

The total number of injected NR electrons in the whole measurement range is $(2.7 \pm 0.6) \times$

[4]The loss of coverage is due to the fact that the magnetic field vector aligns with the spin axis direction at 17:35 UT; then, all sectors are scanning approximately the same μ range.

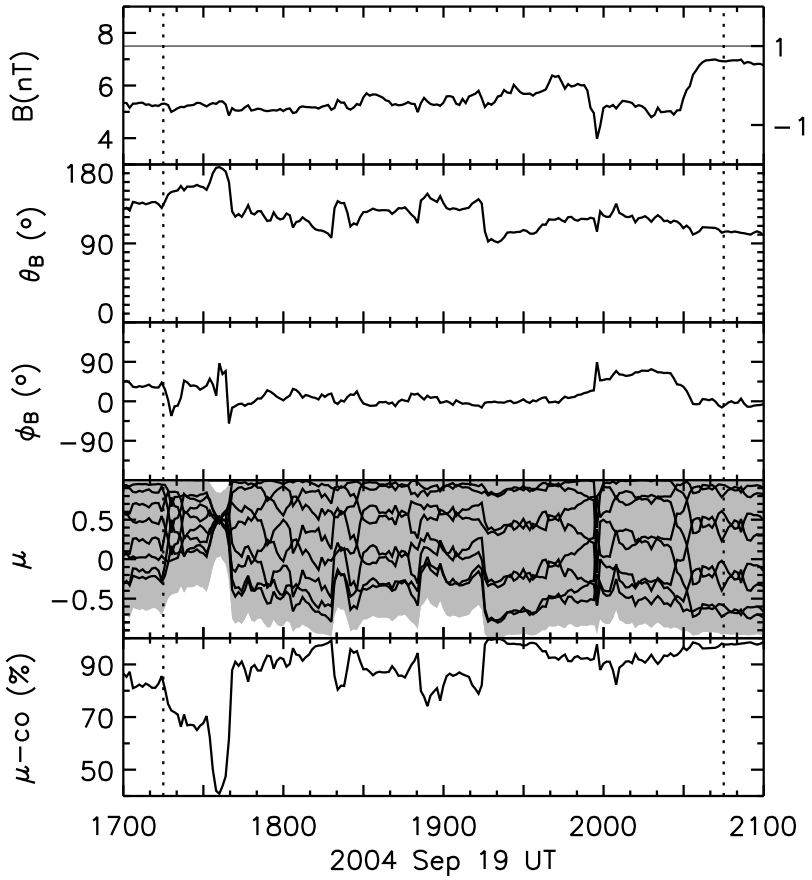

Figure 6.2: Sep04 event: IMF components in the spacecraft coordinate system; μ-range scanned by the LEFS60 telescope (gray area) and pitch-angle cosine of each sector; μ-co. Same presentation as in Figure 5.2.

10^{34}, as determined by the normalization of fitting. By integrating the injection function over time for each energy channel, we can construct the time integrated spectrum which corresponds to a piecewise normalized power-law spectrum with the assumed spectral index of $\gamma_s = 2.6$ in each energy channel. As the total number of electrons in the E'2 channel is slightly lower than what the assumed spectral index would demand, the spectrum can be best fit by a single power-law index if we take $\gamma_s = 2.2$.

The two lower panels in Figure 6.4 compare the timing of the electron injection with the electromagnetic emissions observed at 1 AU. These plots show, from top to bottom, the soft (1.5–12 keV) and hard (25–50 keV) X-ray flux observed by *GOES*/XRS and *RHESSI* and the radio flux observed by *Wind*/WAVES. No CME height-time plot is included in the figure, since there were no images from the C2 coronagraph. Comparing the times of the electron injection with electromagnetic emissions, we see that the start of the electron injection coincides with the peak of soft X-ray emission. No injection episode is observed in accordance with the hard X-rays burst.

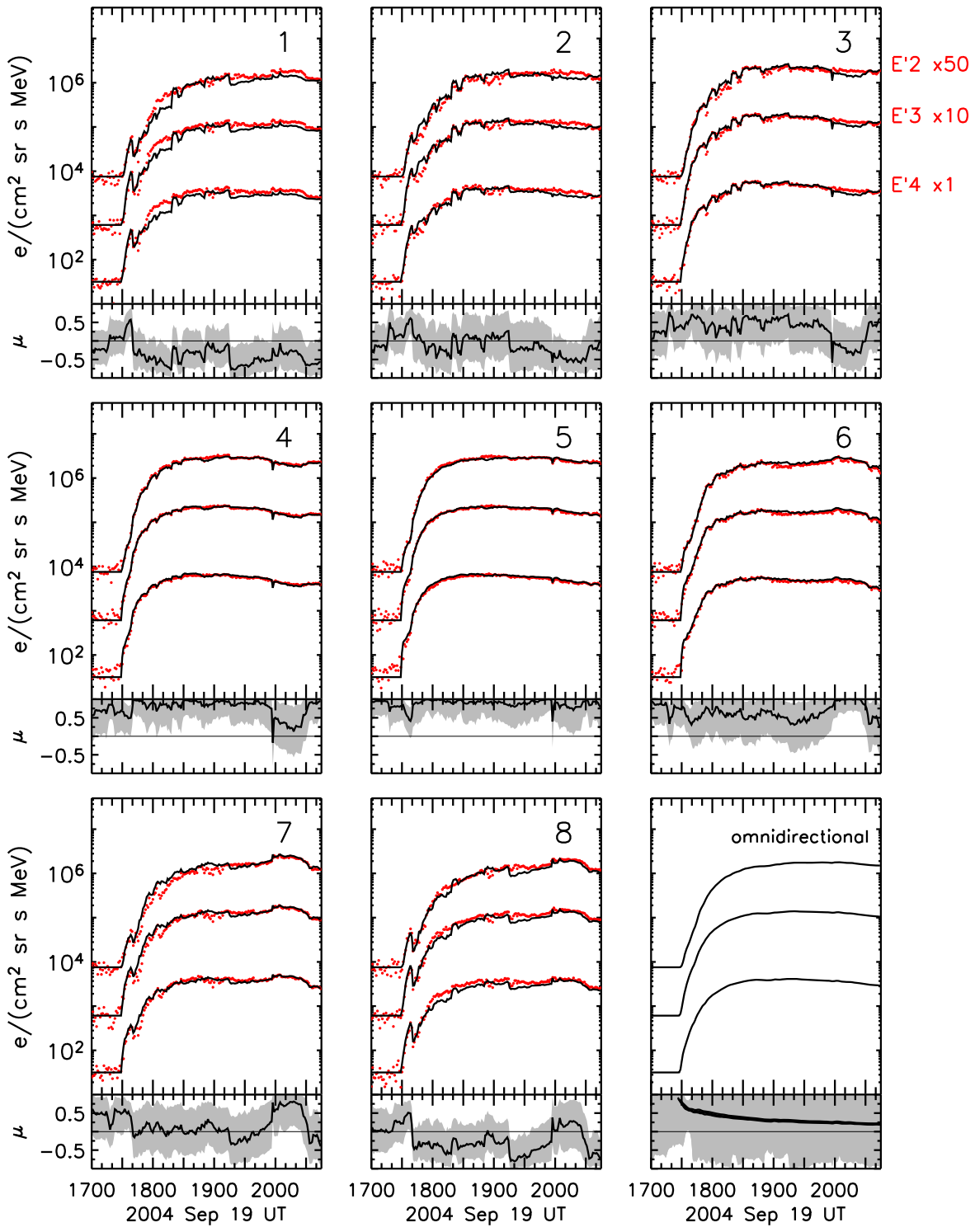

Figure 6.3: Sep04 event: Observational (red dots) and simulated (black line) sectored intensities. Same presentation as in Figure 5.4.

Table 6.1: Results of the fit

Scattering case	ζ {E'2, E'3, E'4}	λ_r (AU)
Isotropic scattering	{10, 13, 13} = 36	0.2
μ-dep with $\epsilon = 0.10$	{13, 13, 12} = 38	0.2
μ-dep with $\epsilon = 0.01$	{15, 15, 13} = 43	0.2

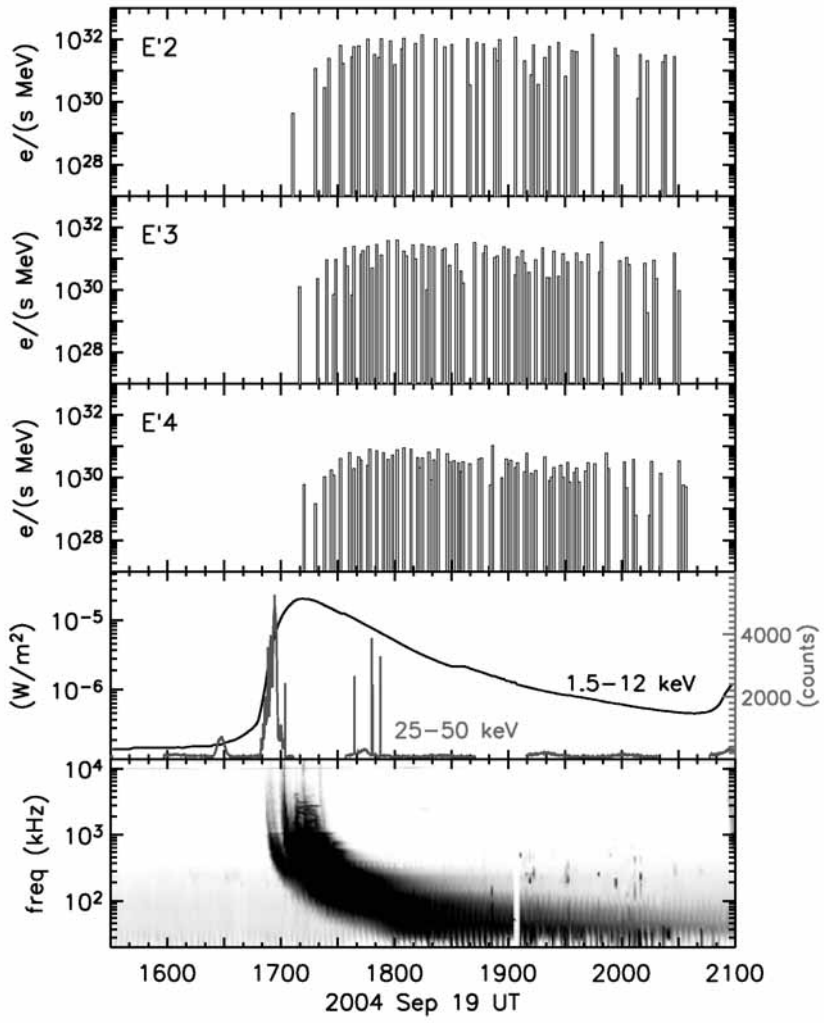

Figure 6.4: From top to bottom: Derived NR electron injection profiles for the three modeled energy channels (injection times are shifted by 8 min to account for the light travel time). Soft (black line; left axis) and hard (gray line; right axis) X-ray flux profiles. Radio flux observed by Wind/WAVES.

The beginning of the injection is also coincident with a set of multiple type III bursts observed by *Wind*/WAVES between 16:55 UT and 17:30 UT (fifth panel in Figure 6.4). While the deconvolved injection extends to at least three hours, the type III emission seen by *Wind*/WAVES lasts ~35 min. A very sporadic type II was reported in association with this SEP event between 17:15 UT and 18:15 UT (from *Wind*/WAVES internet site); but it is not visible in Figure 6.4.

Therefore, we conclude that the most plausible scenario to explain this event is that electrons are provided by a CME-driven shock because: (i) there is a time-extended injection of electrons; (ii) a sporadic 2.5–14 MHz type II burst was observed between 17:15 UT and 18:15 UT; and (iii) a CME was observed by *SOHO*/LASCO at 22:42 UT.

6.2 The 2001 December 26 event

6.2.1 Electromagnetic emissions

The SEP event observed on 2001 December 26 (DOY 360) has been related to an impulsive M7.1 flare (onset at 04:32 UT and maximum at 05:40 UT) observed in association with an Hα flare at N08W54 (Cane et al. 2006).

A fast CME, with plane-of-sky speed of 1446 km s^{-1} and a width of 212°, was first seen by the LASCO C2 coronagraph at 05:30 UT. Cane et al. (2006) reported the passage of an interplanetary shock at *ACE* around 04:41 UT on December 29 (DOY 363) with a transit speed of 570 km s^{-1} (shock transit time from the Sun to 1 AU of 73 h).

Cane & Erickson (2005) examined the radio data observed on December 26 by *Wind*-/WAVES in conjunction with ground-based data from the Culgoora radio observatory (Prestage et al. 1994) and BIRS[5] (Erickson 1997). Figure 6.5 shows the associated radio emission observed by *Wind*/WAVES and BIRS for an extended time period of 19 hours. Type III emission started around 05:15 UT and lasted for approximately 5 min. Cane & Erickson (2005) reported a very strong continuation of a metric type II burst, showing a clear extension to relatively low frequencies and clear fundamental and harmonic bands between 17:00 UT and 21:00 UT near 0.2 and 0.4 MHz. These authors pointed out that this type II emission was probably related to the CME-driven shock.

[5]BIRS (Bruny Island Radio Spectrometer); `http://fourier.phys.utas.edu.au/birs/`

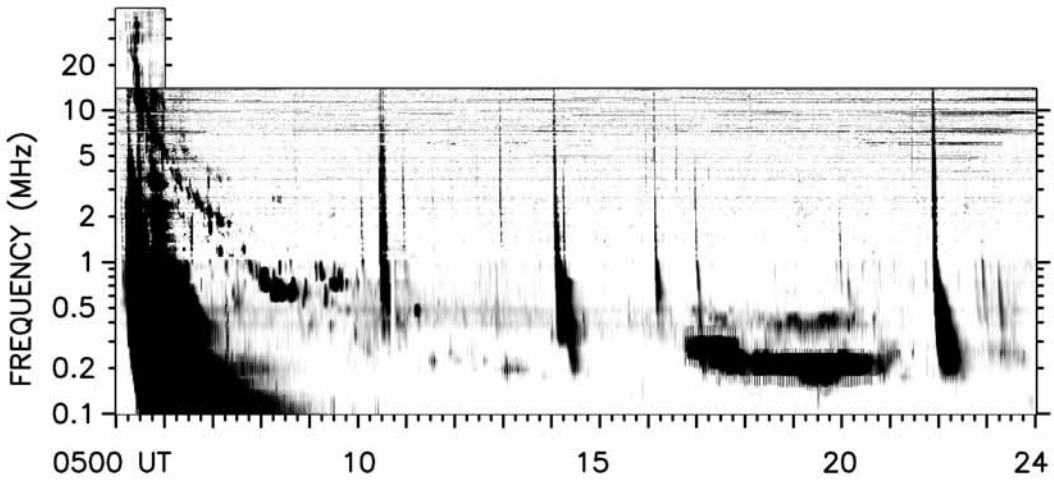

Figure 6.5: Dec01 event: Radio emission on 2001 December 26 observed below 14 MHz by Wind/WAVES and from 14 to 57 MHz by BIRS. Type III emission is seen at the beginning of the event. Fundamental and harmonic bands of type II are also seen extending to about 0.15 MHz (from Cane & Erickson 2005).

6.2.2 In-situ energetic particles

Figure 6.6 shows the spin-averaged 62–312 keV electron intensities observed by the EPAM-/LEFS60 telescope from December 21 (DOY 360) to December 25 (DOY 364). The first NR electrons were detected above the pre-event background at 05:27 UT in the E'4 channel. The maximum spin-averaged intensity was observed at 06:51 UT in the three energy channels. We will study this event from 05:30 UT to 09:00 UT (gray area in Figure 6.6). For comparison, in the top panel of Figure 6.6 we show the DE30 electron intensities (thin line). The similarity of the trends during the selected time period suggests that there is negligible ion contamination in the LEFS60 NR electron profiles.

For completion, the top panel of Figure 6.6 also includes the 8-min spin-averaged proton intensities observed by the LEMS120 telescope and by the ERNE telescope (thin line) between 1 and 5 MeV approximately[6]. As can be seen, the onset of the proton event observed at *ACE* occurs shortly after the onset of the NR electron event and shows a prompt rise. The onset of the 1.33–4.75 MeV proton event observed by ERNE is registered ~90 min after the onset of the NR electron event, as expected[7]. The early onset at *ACE* suggests that this portion of the proton event is most likely contaminated by faster particles from the onset of the

[6]In Figure 6.6, the ERNE measurements in the low energy channel (1.33–1.90 MeV) are multiplied by a factor of 5, whereas measurements in the high energy channel (1.90–4.75 MeV) are multiplied by 0.5.

[7]Under scatter-free conditions, one 312 keV electron spends ~12 min to travel from 2 $R_\odot$ to 1 AU along a nominal Parker spiral IMF line (if u = 400 km s^{-1}), whereas a 4.8 MeV proton needs ~96 min to reach the same position. Thus, if both particles are released simultaneously, they will be observed at 1 AU with 84 min time difference.

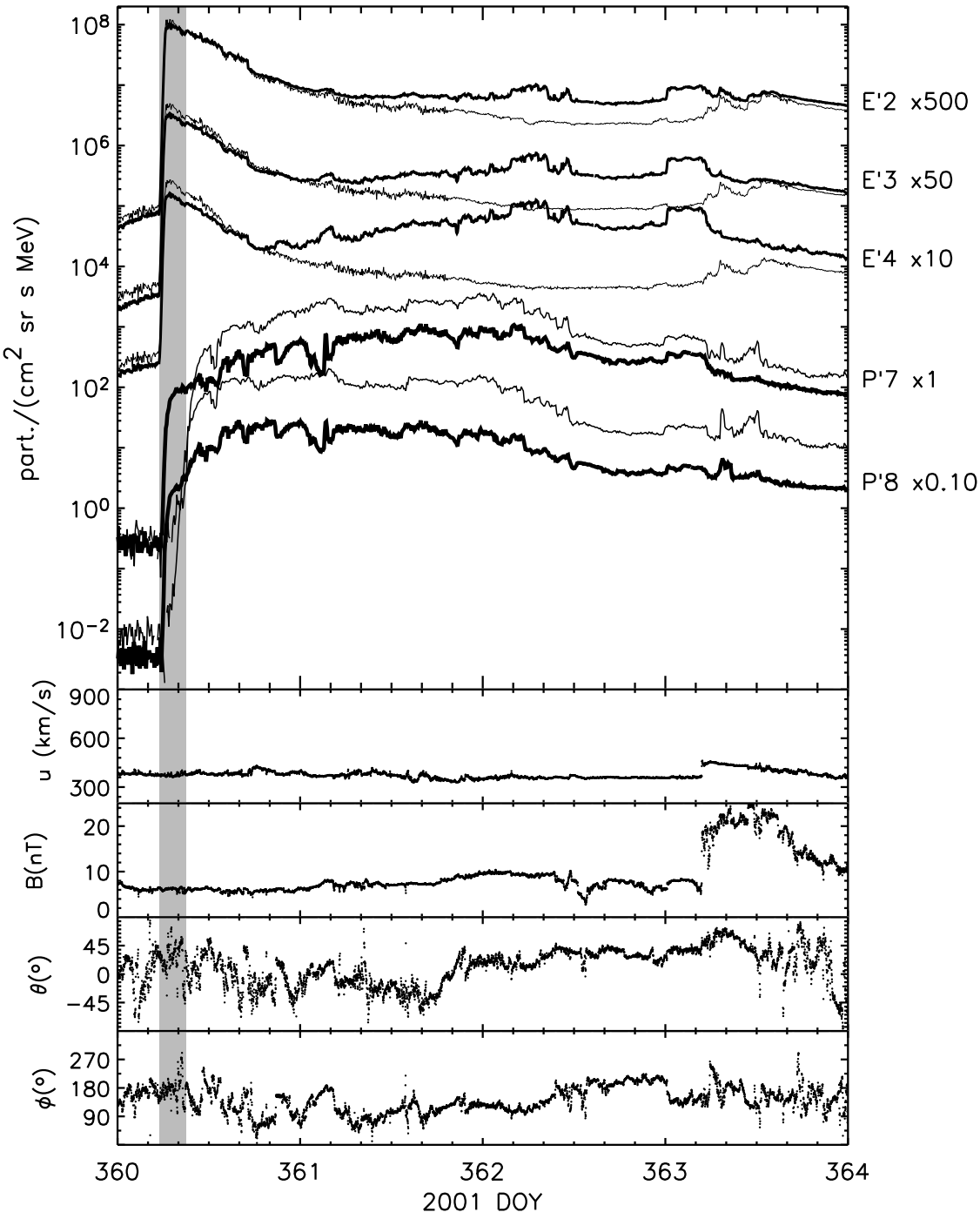

Figure 6.6: Dec01 event: Particle event, solar wind and magnetic field components in the RTN coordinate system. Same presentation as in Figure 5.1.

NR electron event up to approximately ~20:00 UT on DOY 360 when electron intensities decrease and proton intensities at both ACE/LEMS120 and SOHO/ERNE increase, tracking each other. After 20:00 UT on DOY 360, NR electron intensities observed by the LEFS60 telescope mimic the proton intensity profiles. DE30 electron intensities do not show such behavior, which suggests that the LEFS60 channels are contaminated by energetic protons after this time.

Cane et al. (2006) studied the event-averaged abundance of Fe relative to O at energies above 25 MeV nucl^{-1}, from 360/05:30 UT to 362/22:42 UT, and reported a ratio of Fe/O = 4.94 ± 0.10. Therefore, they concluded that this SEP event contained a significant contribution from flare-accelerated particles.

The four lower panels of Figure 6.6 show the solar wind velocity and the three components of the IMF in the RTN spacecraft coordinate system. SWEPAM data indicate that during the NR electron event, *ACE* was embedded in a solar wind stream with a mean velocity 374 km s^{-1}. Both the solar wind velocity and the IMF direction were stable throughout the NR electron event. Therefore, the Parker IMF model and the approximations adopted in the model for particle propagation are reasonable assumptions. The nominal footpoint of the field line connecting *ACE* to the Sun was at W64, as estimated from the observed solar wind speed, which was close to the longitude of the flare site (W54). The spectral index of the derived differential intensity spectrum is $\gamma = 2.5$, so we take $\gamma_s = 3.0$ as a first approximation of the spectral index of the electron source (see section 3.6).

6.2.3 Deconvolution of the NR electron event

Figure 6.7 shows the *ACE*/MAG magnetic field measurements in the spacecraft coordinate system, the range of μ-values scanned by the LEFS60 telescope and the μ-co of the telescope for the period under study. As can be seen, the IMF polarity is negative during most of the selected time period, with sporadic reversals after 08:00 UT. The μ-co of the telescope varies between 40% and 100%, with a mean coverage μ-co ~76%. As the telescope scans particles coming field aligned (gray area in panel four) and μ-co $\geq$ 70%, the sectored data ensures a detailed description of the NR electron event.

We simulate this electron event following the procedure described in section 5.2.3 for the May00 event. We exclude from the fits those data points associated with the period of reversed polarity (+1). The lowest values of ζ obtained for each scattering case are listed in Table 6.2. Figure 6.8 shows the case with the lowest ζ. Blue dots mark the points excluded from the fit due to the change of polarity in the IMF.

The best fit is obtained by taking $\lambda_r = 0.20$ AU and μ-dependent scattering with $\epsilon = 0.01$.

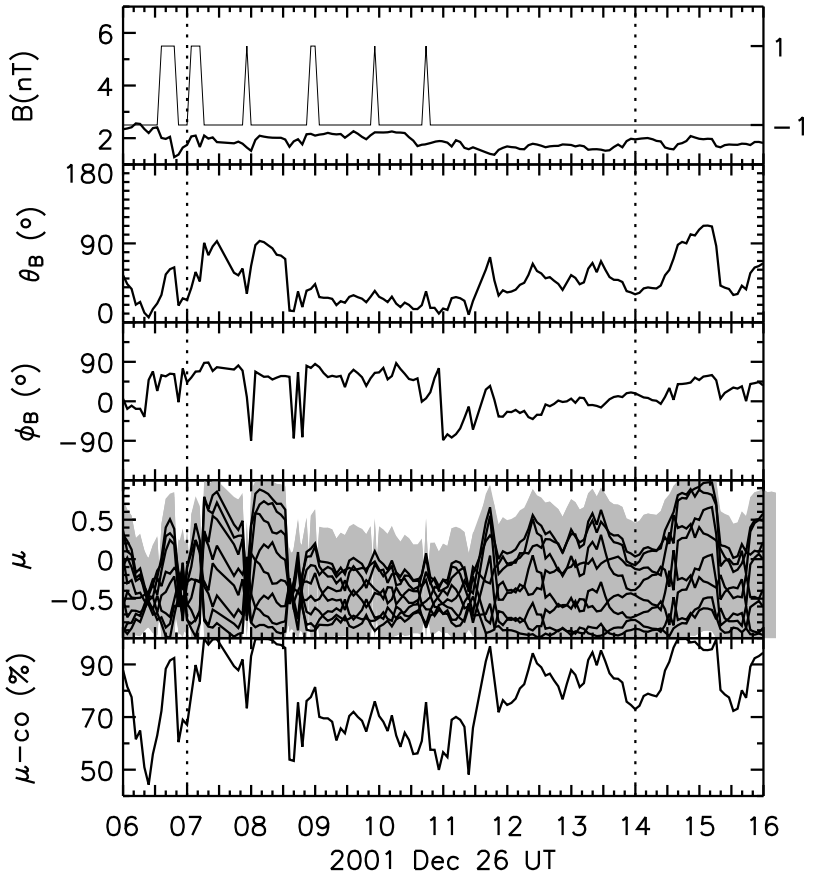

Figure 6.7: Dec01 event: IMF components in the spacecraft coordinate system; μ-range scanned by the LEFS60 telescope (gray area) and pitch-angle cosine of each sector; μ-co. Same presentation as in Figure 5.2.

The fit succeeds in reproducing the sectored intensity profiles for the entire period. Differences between the simulated and measured sectored intensities appear mainly between 08:20 and 08:30 UT (that is, during the period of reversed polarity) and suggest that the injection history and/or the interplanetary transport conditions of the NR electrons might have been different in the flux tubes with opposite IMF polarity.

The values of the solar electron injection derived from the best fit are shown in the three top panels of Figure 6.9 (for convenience of comparison with the observed solar electromagnetic emissions, electron injection times are shifted by 8 min to account for the light travel time). The injection profile clearly shows one single component starting around 05:20 UT, nearly simultaneous in the three energy channels, and lasting at least three hours. The total number of injected NR electrons in the whole measurement range is $(1.4 \pm 0.3) \times 10^{35}$, as determined by the normalization of fitting.

By integrating the injection function over time for each energy channel, we find that the

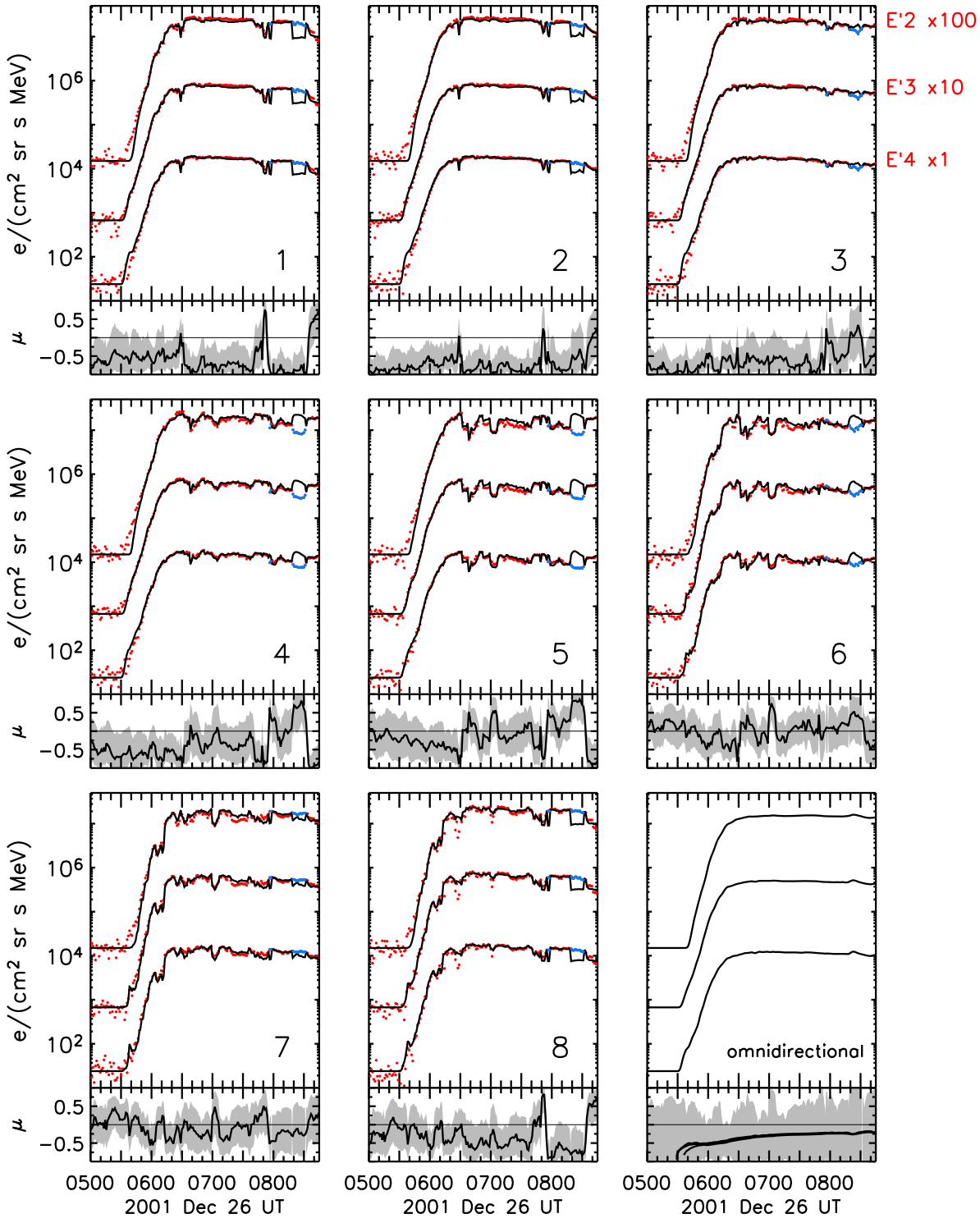

Figure 6.8: Dec01 event: Observational (red dots) and simulated (black line) sectored intensities. Blue dots indicate the data points excluded from the fit due to the reversal of polarity of the IMF. Same presentation as in Figure 5.4.

Table 6.2: Results of the fit

Scattering case	ζ {E'2, E'3, E'4}	λ_r (AU)
Isotropic scattering	{ 6, 9, 15} = 30	0.2
μ-dep with $\epsilon = 0.10$	{10, 5, 10} = 25	0.2
μ-dep with $\epsilon = 0.01$	{13, 4, 7 } = 24	0.2

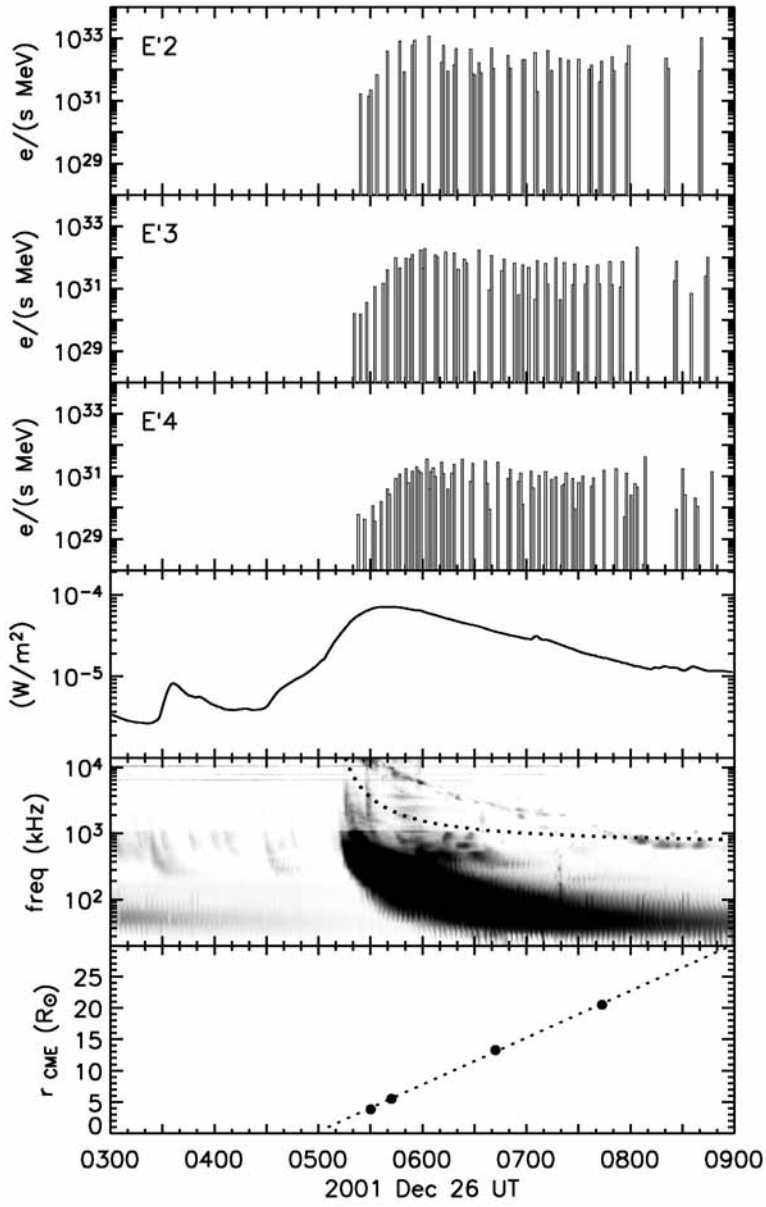

Figure 6.9: Dec01 event: Electron injection and associated electromagnetic emissions. Same presentation as in Figure 5.5.

source spectrum can be best fit by a power-law with index $\gamma_s = 2.6$, as the total number of electrons in the E'2 channel is a bit lower than what the assumed spectral index ($\gamma_s = 3.0$) would demand.

The three lower panels in Figure 6.9 compare the timing of the electron injection with the electromagnetic emissions observed at 1 AU. These plots show, from top to bottom, the soft X-ray flux observed by *GOES*/XRS, the radio flux observed by *Wind*/WAVES and the CME height-time plot from *SOHO*/LASCO Catalog. Comparing the times of the electron injection to the electromagnetic emissions, we see that the electron injection starts during the rising phase of the soft X-ray event and that the maximum injection intensity is reached at 06:00 UT, 20 min after the soft X-ray peak flux. The beginning of the injection coincides with the beginning of the type II burst emission at 14 MHz. This emission is consistent with being originated from a source from behind the CME leading edge if the density model of Mann et al. (1999) is assumed (dotted line in the fifth panel). Some bursts observed after 08:00 UT seem to originate from the CME leading edge itself. Thus, it is plausible that NR electrons observed during the rising phase of this event were provided by the CME-driven shock.

In this scenario, the source injecting NR electrons into the interplanetary medium must have moved from 2 $R_\odot$ to 30 $R_\odot$ during the period from 05:00 to 09:00 UT. However, the model assumes that the source is fixed at 2 $R_\odot$. We can estimate the influence of a moving source on the interpretation of the results by studying the difference in propagation time that a change in the location of the source would introduce. The left panel of Figure 6.10 shows the time that an electron spends propagating field aligned from 2 $R_\odot$ to 1 AU as a function of the electron energy (50–350 keV); assuming a nominal Parker spiral IMF line with $u = 374$ km s^{-1}. The time difference to be considered if the source is instead located at 15 $R_\odot$ or at 30 $R_\odot$ is shown in the right panel of Figure 6.10. The dotted horizontal line marks the 72-s time resolution used for the observational data. If the source was located at 30 $R_\odot$ instead of being at 2 $R_\odot$, modeled intensities would be delayed by a maximum of 2.5 min in the E'2 channel (62–102 keV) and the delay would be greater than the observational time resolution for the whole energy range. On the other hand, if the source is located closer to the Sun than 15 $R_\odot$, the delay introduced by assuming the source located at 2 $R_\odot$ would be smaller than the used time resolution of the observational data. As already pointed out, the type II radio emission seems to be consistent with being originated from a source from behind the CME leading edge, which is observed at 30 $R_\odot$ at 09:00 UT. Therefore, we conclude that the derived electron injection profile is reliable before 07:00 UT (when the leading edge of the CME is at heights lower than 15 $R_\odot$). After 07:00 UT, the delay is smaller than 3 min (~1.5 min at 312 keV) and after ~180 min of electron injection, it does not represent a noticeable error in the scenario depicted.

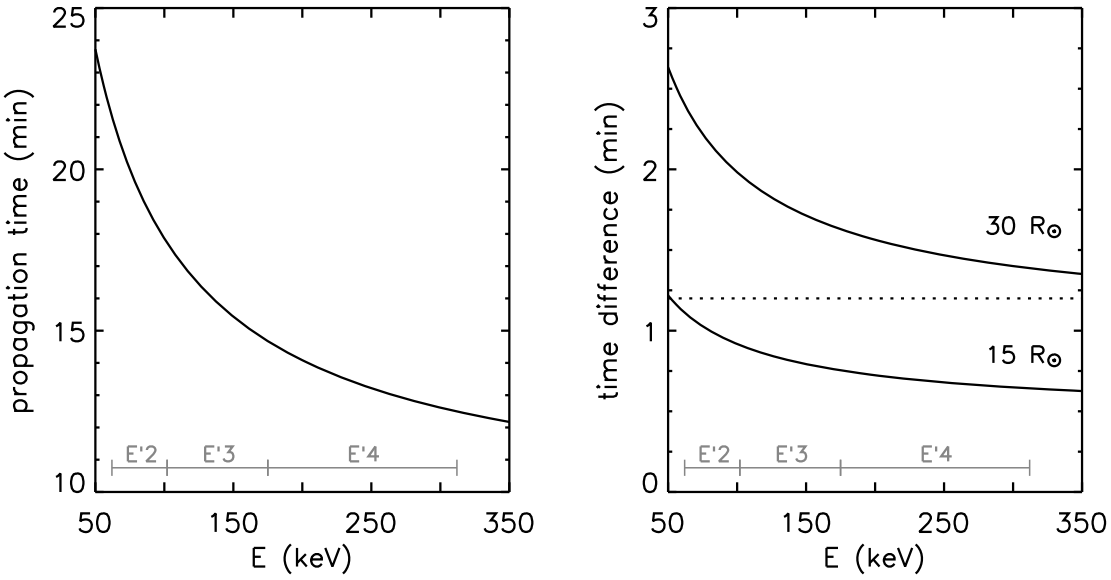

Figure 6.10: Propagation time between 2 $R_\odot$ and 1 AU plotted versus the energy of the electron (left). Time difference when the source is located at 15 $R_\odot$ or at 30 $R_\odot$ (right). The dotted horizontal line marks the 72 s time resolution of the observational data. The energy range of each channels is indicated in gray.

6.3 The 1998 May 27 event

6.3.1 Electromagnetic emissions

Three active regions were observed near the time of the onset of the NR electron event observed on 1998 May 27 (Torsti et al. 2002). Three Hα flares were observed with maximum emission at 13:00 UT, at 13:28 and at 13:38 UT in AR 8226 (N18 W60), at 13:33 UT in AR 8224 (S12W80) and at 13:35 UT in AR 8227 (N22 E51). The soft X-ray flux observed by *GOES* started to rise at 13:15 UT, and a C7.5 flux peak was observed at 13:35 UT. Around 13:30 UT (±5 min) *Yohkoh*/SXT observed the region AR 8226 and surroundings in flare mode, and saw plasma flows along large loop structures (Torsti et al. 2002).

Klein et al. (2005) reported a fast (~880 km s^{-1}) CME, first seen in LASCO C2 images at 13:45 UT with central position angle 175° and angular width 268°, at a projected distance from the Sun center of about 4 $R_\odot$. However, Torsti et al. (2002) derived a central position angle of 304° from the analysis of the same images. Figure 6.11 shows the full-disk *Yohkoh*/SXT pre-flare image at 12:28 UT, together with the active region locations and the coronal mass ejection observed by LASCO.

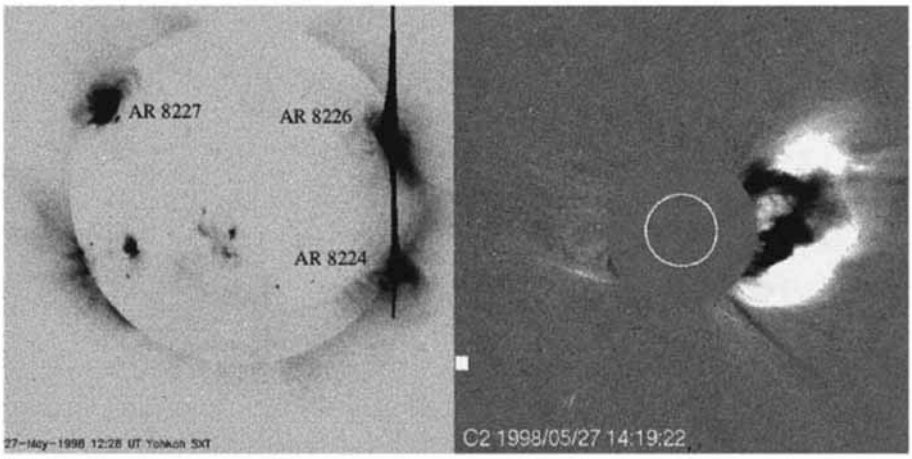

Figure 6.11: May98 event: Yohkoh/SXT full-disk image on 1998 May 27 at 12:28 UT (left) showing the active regions AR 8226, AR 8224, and AR 8227. Difference image of the CME at 14:19 UT (right). Note the large trans-equatorial soft X-ray loop connecting AR 8226 and AR 8224 just below the CME observed by LASCO (from Torsti et al. 2002).

The EIT 195 Å running difference images showed brightenings propagating away from AR 8226, starting at 13:06 UT, indicating a coronal EIT wave propagating away from AR 8226 concurrently with the CME lift-off (Torsti et al. 2002). In close temporal association, a type IV radio burst was observed by the Nançay Radioheliograph, from 13:10 to 13:40 UT (Klein et al. 2005). Torsti et al. (2002) associated the type IV radio burst with emission coming from the large scale loop system over the solar northwestern limb. Type III radio emission dominated from 13:14 UT to 13:30 UT in the frequency range below 70 MHz (Klein et al. 2005). *Wind*/WAVES registered a weak and intermittent 4–1 MHz type II burst from 13:30 to 14:20 UT, which might correspond to a shock traveling from ~3.5 $R_\odot$ to 10 $R_\odot$ (Torsti et al. 2002).

6.3.2 In-situ energetic particles

Figure 6.12 shows spin-averaged 62–312 keV electron intensities observed by the EPAM-/LEFS60 telescope from 1998 May 27 (DOY 147) to May 30 (DOY 150). The first NR electrons were detected above the pre-event background at 13:30 UT in the E'4 channel. The maximum spin-averaged intensity was observed at 14:27 UT in the E'4 channel, at 14:29 UT in the E'3 channel and at 14:30 UT in the E'2 channel. We will study this event from 13:30 UT to 17:30 UT (gray area in Figure 6.12). For comparison, the top panel of Figure 6.12 shows the DE30 electron intensities (thin line). The similar trends indicate that there is negligible ion contamination in the LEFS60 NR electron profiles during the selected time interval.

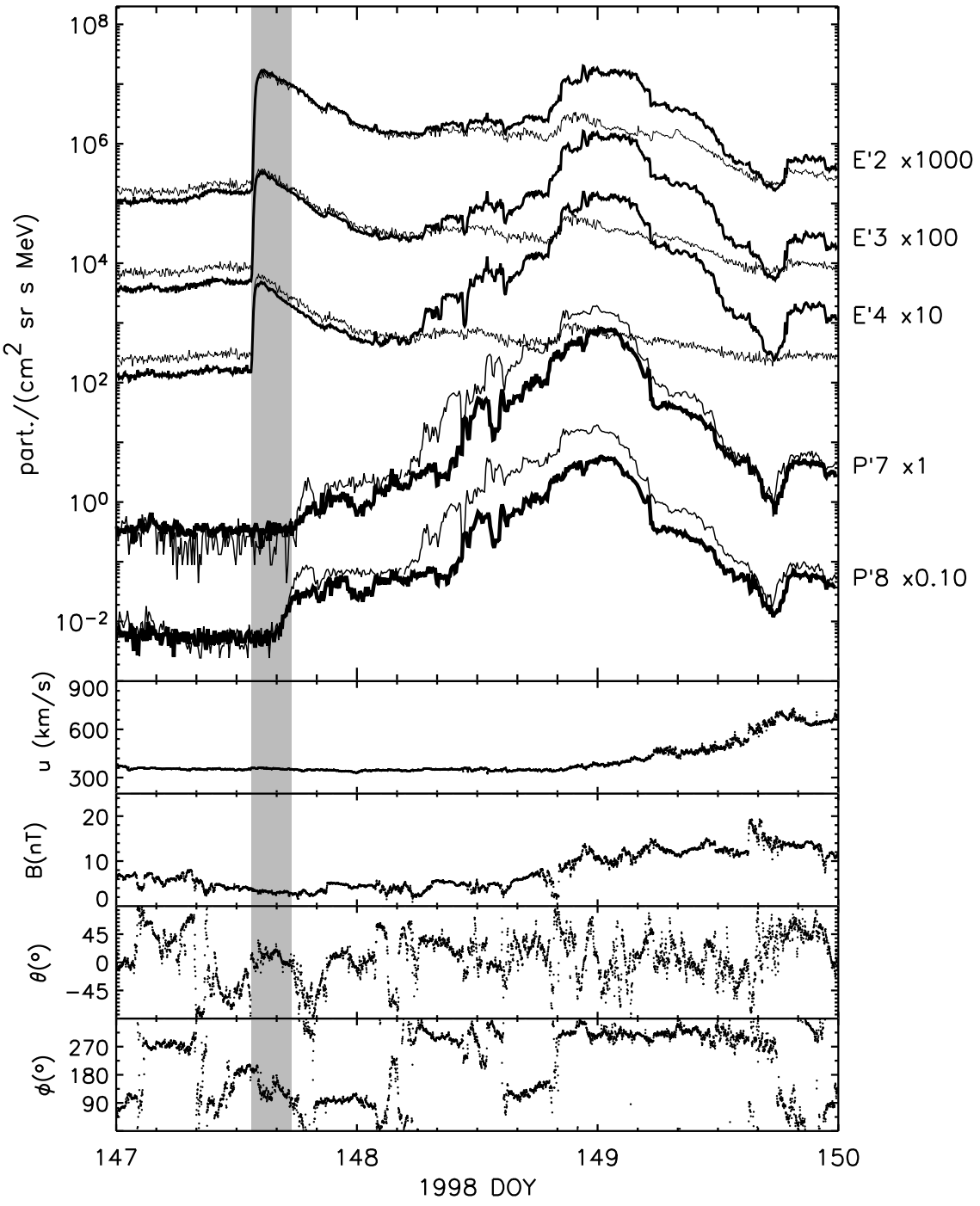

Figure 6.12: May98 event: Particle event, solar wind and magnetic field components in the RTN coordinate system. Same presentation as in Figure 5.1.

For completion, the top panel of Figure 5.7 also includes the 8-min spin-averaged proton intensities observed by the LEMS120 telescope and by the ERNE telescope (thin line) between 1 and 5 MeV approximately[8]. The onset of the proton event is observed ~90 min after the onset of the NR electron event. Thus, we conclude that the onset phase of the proton intensity profiles is not contaminated by faster particles. Note that after 06:00 UT on DOY 148 the electron profiles mimic the proton profiles. As DE30 electrons do not show this evolution, it is clear that LEFS60 channels are contaminated by energetic protons after this time.

The event was classified as moderately ^{3}He-rich by Slocum et al. (2003), with ^{3}He/^{4}He ~ 0.04 in the 0.5–2.0 MeV nucl^{-1} energy range, estimated during the summing period from 147/09:36 UT to 148/14:24 UT. Torsti et al. (2002) reported a very strong ^{4}He/p ratio enhancement in the beginning of the event (~80%) followed by a high ratio of ~20–30% in the 2.7–60 MeV nucl^{-1} energy range during the ten hour period after the onset of the event.

The lower four panels in Figure 6.12 show the solar wind velocity and the three components of the IMF in the RTN spacecraft coordinate system. SWEPAM data indicate that during the NR electron event *ACE* was embedded in a solar wind stream with a mean velocity of 354 km s^{-1}. The solar wind velocity and the IMF magnitude were stable through the selected time period. The IMF latitude, θ, was ~0° during the whole period. The IMF longitude, ϕ, remained relatively stable, ϕ ~202°, from 13:30 UT to 14:00 UT but it showed some variations afterward. The nominal footpoint of the field line connecting *ACE* to the Sun was at W68, being in between the longitudes of the two western flare sites, W60 and W80. The spectral index of the derived differential intensity spectrum is $\gamma = 3.3$, so we take $\gamma_s = 3.8$ as a first approximation of the spectral index of the electron source (see section 3.6).

6.3.3 Deconvolution of the NR electron event

Figure 6.13 shows the *ACE*/MAG magnetic field measurements in the spacecraft coordinate system, the range of μ-values scanned by the LEFS60 telescope and the μ-co of the telescope for the period under study. From Figure 6.13, it can be seen that the IMF polarity is negative during most of the selected time period; except for a sporadic reversal at 14:00 UT. The μ-co of the telescope varies between 50% and 100% approximately, with a mean coverage of μ-co ~88%. The fact that the telescope scans particles propagating antisunward along the field direction (gray area in panel four of Figure 6.13) in addition to μ-co $\geq$ 70% ensures a detailed description of the NR electron event by the sectored data. During the rising phase of the event, from 13:30 to 14:00 UT, the mean μ-co is ~78%; then, it rises to ~92%.

[8] In Figure 6.12, the ERNE low energy channel (1.26–2.16 MeV) is multiplied by a factor of 5, whereas the high energy channel (2.16–5.12 MeV) is multiplied by 0.5.

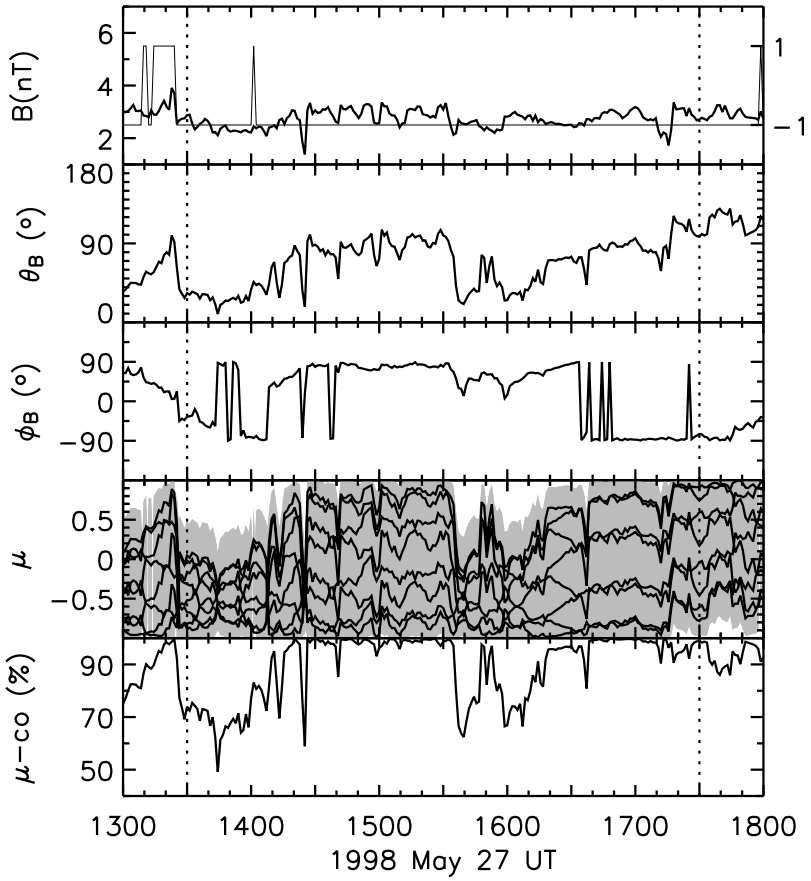

Figure 6.13: May98 event: IMF components in the spacecraft coordinate system; μ-range scanned by the LEFS60 telescope (gray area) and pitch-angle cosine of each sector; μ-co. Same presentation as in Figure 5.2.

We simulate this electron event following the procedure described in section 5.2.3 for the May00 event. The lowest values of ζ obtained for each scattering case are listed in Table 6.3. Figure 6.14 shows the fit for the case with the lowest ζ; it corresponds to $\lambda_r = 0.10$ AU and μ-dependent scattering with $\epsilon = 0.01$. The optimum fit[9] succeeds in reproducing the sector profiles during the rising phase of the electron event. However, after 14:00 UT, there are differences of less than a factor two between the simulated and measured sectored intensities: the simulation underestimates the observed intensity in those sectors which look mainly antisunward (1, 2 and 3); and it overestimates the intensity in those sectors which look in the sunward direction (6, 7 and 8). Moreover, the higher the energy the smaller the differences.

At least two effects could explain these differences: (1) the local changes observed in the direction of the IMF might introduce slight variations in the features of the injected electrons; and (2) the actual scattering processes at work in the interplanetary medium are not perfectly

[9]In order to assure that $\lambda_r = 0.10$ AU is the optimal value of λ_r, we included $\lambda_r = 0.05$ AU in the study. Since $\zeta(\lambda_r = 0.05) \gg \zeta(\lambda_r = 0.10)$, the optimal fit corresponds to $\lambda_r = 0.10$ AU.

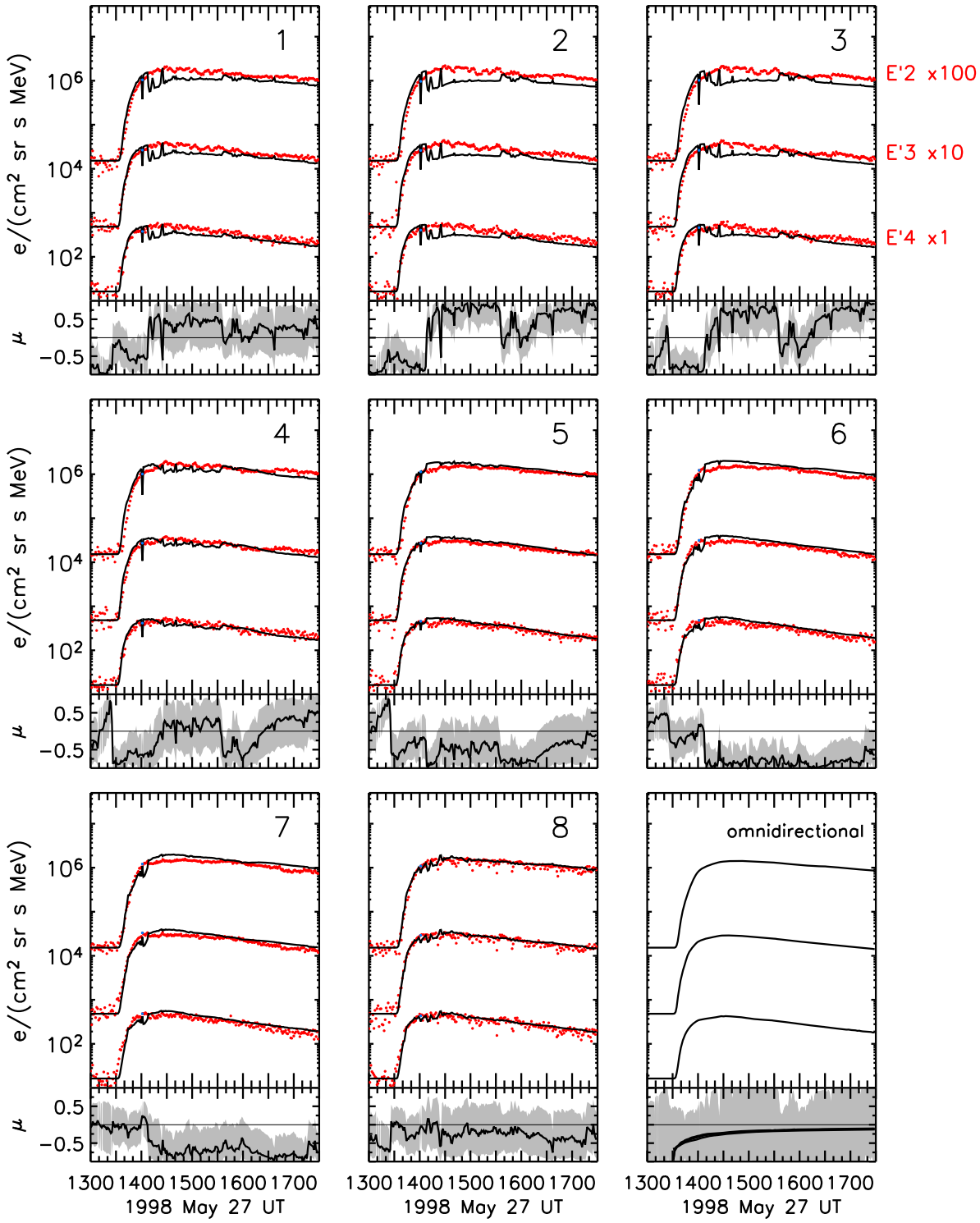

Figure 6.14: May98 event: Observational (red dots) and simulated (black line) sectored intensities. Same presentation as in Figure 5.4.

described by the scattering model. We can also explain these differences by envisioning a radically different scenario. If the actual scenario were a closed loop structure rooted at the bottom of the active region, this would account for the lack of counterstreaming particles predicted by the model after 14:00 UT. If this were the case, particles would be injected at both loop legs and the intensities of particles propagating sunward would be higher at 1 AU. Unfortunately we can not explore this scenario with the present model.

The values of the solar electron injection derived from the best fit are shown in the three top panels of Figure 6.15. The total number of injected NR electrons in the whole measurement range is $(7.3 \pm 0.5) \times 10^{33}$, as determined by the normalization of fitting. At high energies (channel E'4) the injection profile shows three injection components. The first injection episode starts at 13:20 UT, lasts ~20 min and it represents ~80% of the whole injection. A second weaker (~16%) prompt episode can be identified starting at 14:00 UT and lasting ~10 min. A third even weaker injection episode (~4%) begins at ~15:00 UT and lasts ~1 min. At lower energies (channels E'3 and E'2) the injection profiles also show several injection episodes, although it is difficult to identify them as clearly as for E'4. By integrating the injection function over time for each energy channel, we find that the source spectrum can be best fit by a power-law with index $\gamma_s = 3.6$.

The three lower panels in Figure 6.15 compare the timing of the electron injection with the electromagnetic emissions observed at 1 AU. As can be seen, the first electron injection episode starts with the onset of the first type III radio burst at ~13:20 UT, in coincidence with a peak in the hard X-ray flux profile and the rise of the soft X-ray flux. The timing of the second injection component is a bit more uncertain because it starts later than the second weak type III burst observed at 13:45 UT. Torsti et al. (2002) reported a weak and intermittent type II burst from 13:30 UT to 14:20 UT that could be associated with the second injection episode. There is no observational counterpart associated with the weak injection episode observed at ~15:00 UT. The injection episode observed around 15:50 UT seems to be related to small peaks observed in the soft X-rays flux profile[10].

[10]If for this event, the assumed Parker spiral scenario is not correct and instead the particles observed by the spacecraft were traveling along a closed interplanetary loop with injection in both legs, then the second and third injection episodes we have deduced from the deconvolution of the measured sectored intensities may be uncorrect.

Table 6.3: Results of the fit

Scattering case	ζ {E'2, E'3, E'4}	λ_r (AU)
Isotropic scattering	{46, 27, 21} = 94	0.1
μ-dep with $\epsilon = 0.10$	{37, 24, 20} = 81	0.1
μ-dep with $\epsilon = 0.01$	{36, 23, 20} = 79	0.1

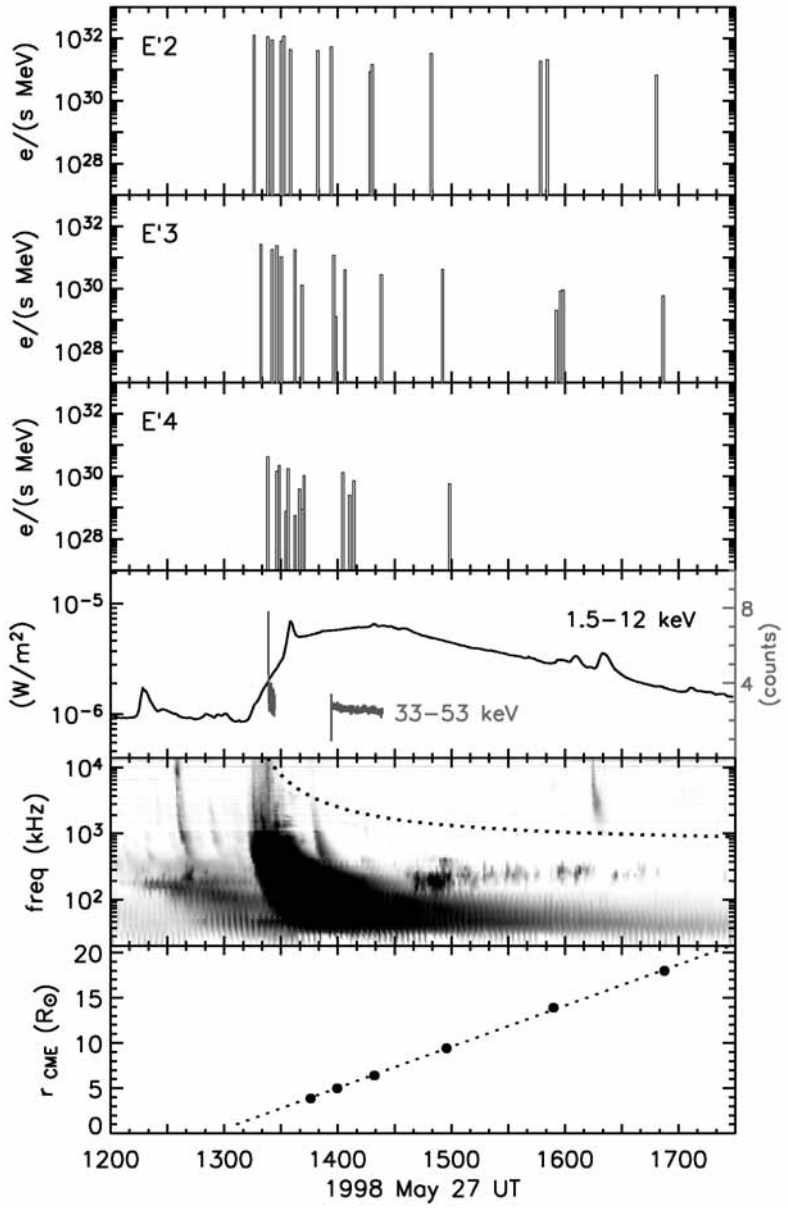

Figure 6.15: May98 event: Electron injection and associated electromagnetic emissions. Same presentation as in Figure 5.5.

6.4 The 2000 July 14 event

6.4.1 Electromagnetic emissions

The SEP event observed on 2000 July 14 is popularly known as the *Bastille Day* event and is associated with one of the largest solar eruptive events of solar cycle 23. This event included a filament eruption, a long-duration X5.7/3B flare, and a fast halo-type coronal mass ejection. Various features of the solar event were observed and studied using data collected by the X-ray, EUV, and white-light imaging telescopes on board the space-borne observatories *Yohkoh*, *SOHO* and *TRACE* as well as with a number of ground-based instruments of different ranges. Many of the results of those studies were published in a special volume of *Solar Physics* (2001, Vol. 204, Issue 1-2).

The main soft-X ray event observed in 2000 July 14 was associated with a filament eruption and an X5.7 flare located at N22W07, AR 9077 (Aulanier et al. 2000; Kosovichev & Zharkova 2001; Smith et al. 2001). Soft X-ray flux began to increase at 10:03 UT, peaked at 10:21 UT and decreased slowly afterwards. A second M3.7 soft X-ray flare occurred in the same region at 13:44 UT. Hard X-ray emission at 33–53 keV started at 10:24 UT and lasted ∼15 min.

The brightest radio emission occurred in close association with the peak of the soft X-ray flux. A group of intense type III bursts, with a particularly bright phase between ∼10:30 UT and 10:40 UT, was seen in *Wind*/WAVES dynamic spectrum (Klein et al. 2001). In addition, there were two other strong type III bursts at ∼12:50 UT and at 13:48 UT (Maia et al. 2001). An extremely broadband, mostly harmonic, 14–0.08 MHz type II radio burst was reported by the *Wind*/WAVES experiment between 10:30 UT and 14:30 UT suggesting the presence of a CME-driven shock wave (Klein et al. 2001).

LASCO provided detailed data on the CMEs associated with the Bastille Day event. After an early event seen in the C2 field of view at about 01:31 UT, a fast halo CME, with plane-of-sky speed of 1674 km s^{-1}, was observed by the LASCO C2 coronagraph at 10:54 UT. The structure was an octopus-like bundle of some magnetic ropes, with the ‘arms’ being connected to several active regions dispersed over almost the whole visible solar surface (Chertok & Grechnev 2005).

6.4.2 In-situ energetic particles

The solar event was accompanied by a large particle flux enhancement in interplanetary space and by a severe geomagnetic storm (D_{st} ∼-300 nT). Neutron monitors showed a rapid rise of relativistic proton fluxes at 1 AU to one of the strongest maximums observed since October

1989 (Klein et al. 2001).

Figure 6.16 shows the spin-averaged 62–312 keV electron intensities observed by the EPAM/LEFS60 telescope from July 14 (DOY 196) to July 17 (DOY 199). The first NR electrons were detected above the pre-event background on 196/10:37 UT in the E'4 channel. The maximum spin-averaged intensity was observed on 197/12:38 UT in the E'4 channel, on 197/12:50 UT in the E'3 channel and on 197/12:50 UT in the E'2 channel. The gray area shows the time period selected for the study, from 196/10:40 UT to 196/13:30 UT. For comparison, Figure 6.16 shows the deflected electron intensities (thin line) with the same scale factors as used for the intensities measured by LEFS60. The similar trends indicate that there is negligible ion contamination in the LEFS60 NR electron profiles during the selected time period.

The E'4 electron intensity rises from a pre-event level of 3×10^3 to a level of 1×10^5 particles $\mathrm{MeV^{-1}cm^{-2}sr^{-1}s^{-1}}$ in one hour, and then it increases by a factor four in the following day. Smith et al. (2001) attributed the slow electron intensity increase to two main effects: (i) interplanetary particle pitch-angle scattering, and (ii) convection of the field lines connecting the spacecraft to different points along the approaching CME-driven shock. These authors rejected the contribution from flare accelerated particles because the spacecraft was assumed to be poorly connected with the flare site (W07).

For completion, the top panel of Figure 6.16 also includes 8-min spin-averaged proton intensities observed by the LEMS120 telescope and by the ERNE telescope (thin line) between 1 and 5 MeV approximately[11]. From the figure, it is clear that the proton intensity profiles observed by LEMS120 are contaminated by faster particles at the onset of the proton event.

Cane et al. (2006) estimated the event-averaged Fe/O ratio at energies above 25 MeV $\mathrm{nucl^{-1}}$, from 196/11:00 UT to 200/19:00 UT, using the *ACE*/SIS instrument and reported a ratio of Fe/O = 0.62 ± 0.14 relative to the coronal value. Therefore, these authors concluded that, on average, this SEP event did not include a significant contribution from flare-accelerated particles.

Smith et al. (2001) identified the passage of three interplanetary shocks at 1 AU, their downstream regions and their CME drivers from DOY 194 to DOY 199. On 195/09:19 UT, *ACE* measured the passage of a first interplanetary shock. Signatures of the passage of the associated interplanetary CME (ICME), including depressed solar wind proton temperature and counter-streaming electrons, were observed from 195/13:00 UT to 196/11:00 UT (Smith et al. 2001). The ICME did not contain the typical IMF rotation characteristic of a magnetic cloud and the ionic composition was typical of slow solar wind. Smith et al. (2001)

[11]The ERNE low energy channel (1.33–1.90 MeV) measurements shown in Figure 6.16 have been multiplied by a factor of 0.03, whereas the high energy channel (1.90–4.75 MeV) has been multiplied by 0.01.

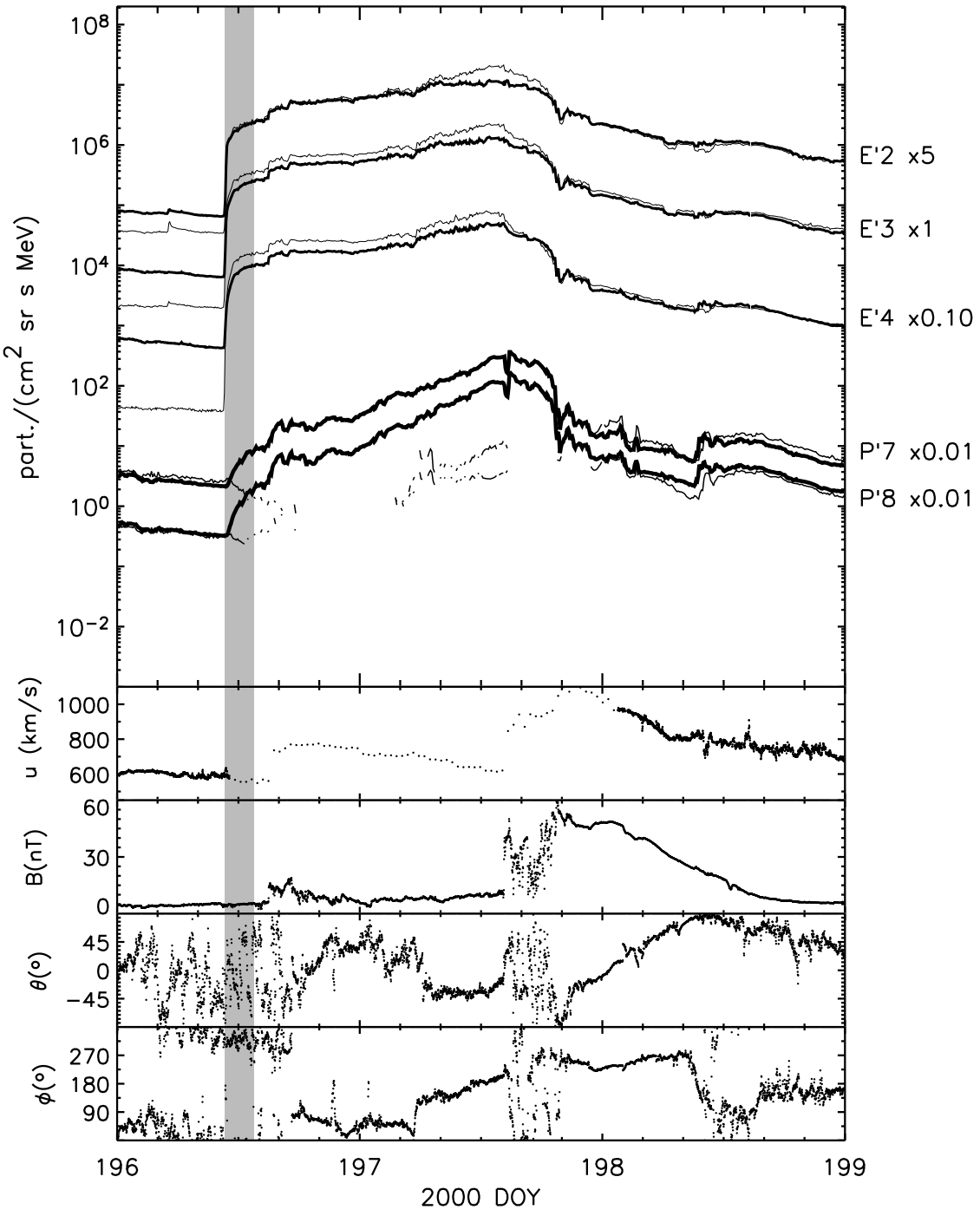

Figure 6.16: Jul00 event: Particle event, solar wind and magnetic field components in the RTN coordinate system. Same presentation as in Figure 5.1.

reported the passage of a second small interplanetary shock on 196/14:59 UT and a third one on 197/14:16 UT. Cane et al. (2006) estimated the passage of the third shock around 197/14:24 UT with an associated transit speed of 1600 km s^{-1}, derived from a shock transit time from the Sun to 1 AU of 26 h. Thus, there was a quiet period in between the tail of the passage of the first ICME and the arrival of the second interplanetary shock, that is, from 196/11:00 UT to 196/14:59 UT, which is roughly the time period selected for the study of the NR electron event.

The lower four panels of Figure 6.16 show the solar wind velocity and the three components of the IMF in the RTN spacecraft coordinate system. Because of high particle backgrounds, SWEPAM data at 64 s time resolution was unavailable from 196/11:00 UT to 198/02:00 UT approximately. Fortunately, search mode SWEPAM data at 33 min time resolution was possible (R. Skoug, 2008, private communication). We assume that during the period under study the average solar wind velocity was 593 km s^{-1}. Thus, the nominal footpoint of the field line connecting *ACE* to the Sun was at W40, 33° away from the longitude of the associated flare site (W07). The spectral index of the derived differential intensity spectrum is $\gamma = 1.6$, so we take $\gamma_s = 2.1$ as a first approximation of the spectral index of the electron source (see section 3.6).

6.4.3 Deconvolution of the NR electron event

Figure 6.17 shows 72-s averaged *ACE*/MAG magnetic field measurements in the spacecraft coordinate system, the range of μ-values scanned by the LEFS60 telescope and the μ-co of the telescope for the period under study. As can be seen, the IMF polarity is positive during most of the period under study with the exception of a reversal in the first 10 min of the event. The μ-co of the telescope varies between 65% and 100%, with a mean coverage μ-co ~87%. As the telescope scans particles propagating antisunward along the field direction (see gray area in panel four) and μ-co $\geq$ 70%, sectored data provides a detailed description of the NR electron event.

We simulate this electron event following the procedure described in section 5.2.3 for the May00 event. We exclude from the fits the data points associated with the period of reversed polarity (-1). The lowest values of ζ obtained for each scattering case are listed in Table 6.4. Figure 6.18 shows the case with the lowest ζ. Blue dots mark the points excluded from the fit due to the change of polarity in the IMF.

The best fit[12] is obtained by taking $\lambda_r = 0.10$ AU and isotropic scattering. This fit succeeds

[12]In order to assure that $\lambda_r = 0.10$ AU is the optimal value of λ_r, we had to include $\lambda_r = 0.05$ AU in the study. Since ζ was higher for the latter, we were able to confirm that the optimal fit corresponds to $\lambda_r = 0.10$ AU.

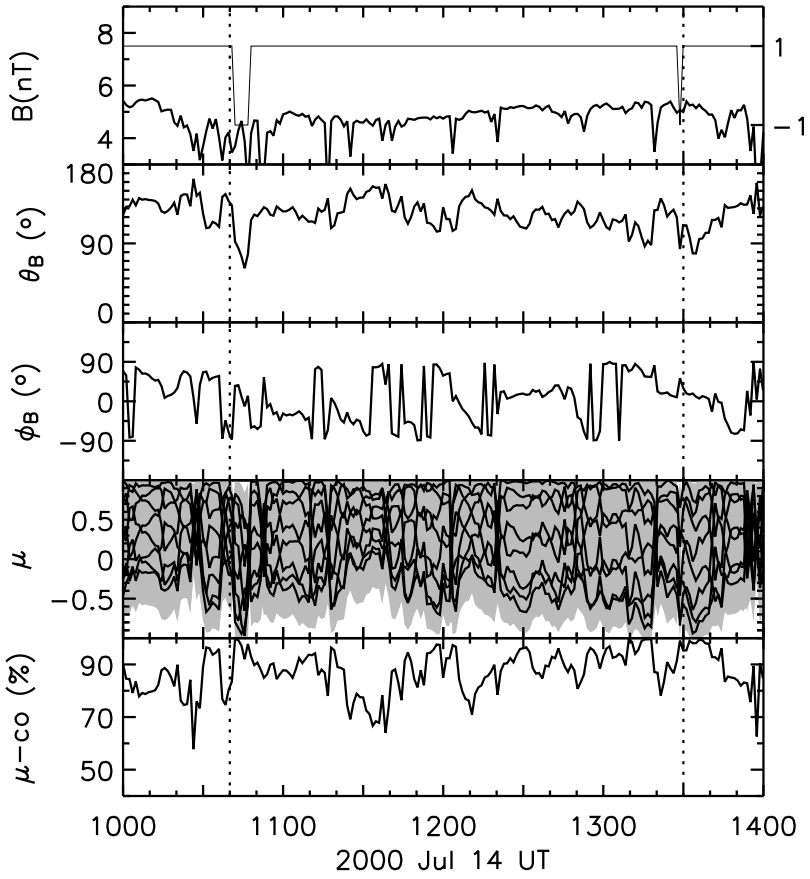

Figure 6.17: Jul00 event: IMF components in the spacecraft coordinate system; μ-range scanned by the LEFS60 telescope (gray area) and pitch-angle cosine of each sector; μ-co. Same presentation as in Figure 5.2.

in reproducing the sectored intensity profiles, with the exception of a short period between 10:40 and 10:50 UT, where there is a factor of two of difference between the observations and the simulated profiles. Differences are probably due to the change of polarity of the IMF and may indicate that the injection history and/or the interplanetary transport conditions were slightly different in the flux tubes with opposite IMF polarity.

The values of the solar electron injection derived from the best fit are shown in the three top panels of Figure 6.19. The injection profile starts at 10:27 UT, at 10:30 UT and at 10:34 UT in the E'2, E'3 and E'4 energy channels, respectively, and it extends in time for at least 3 h. The injection profile clearly shows two components: one prompt (∼1 min) component followed by a second time-extended component starting after 10:50 UT. The total number of injected NR electrons in the whole measurement range is $(3.5 \pm 0.7) \times 10^{35}$, as determined by the normalization of fitting. Although the prompt injection is larger in magnitude than the extended injection, it only represents ∼28% of the whole injection profile, and this contribution would be even smaller if we were studying the whole electron event.

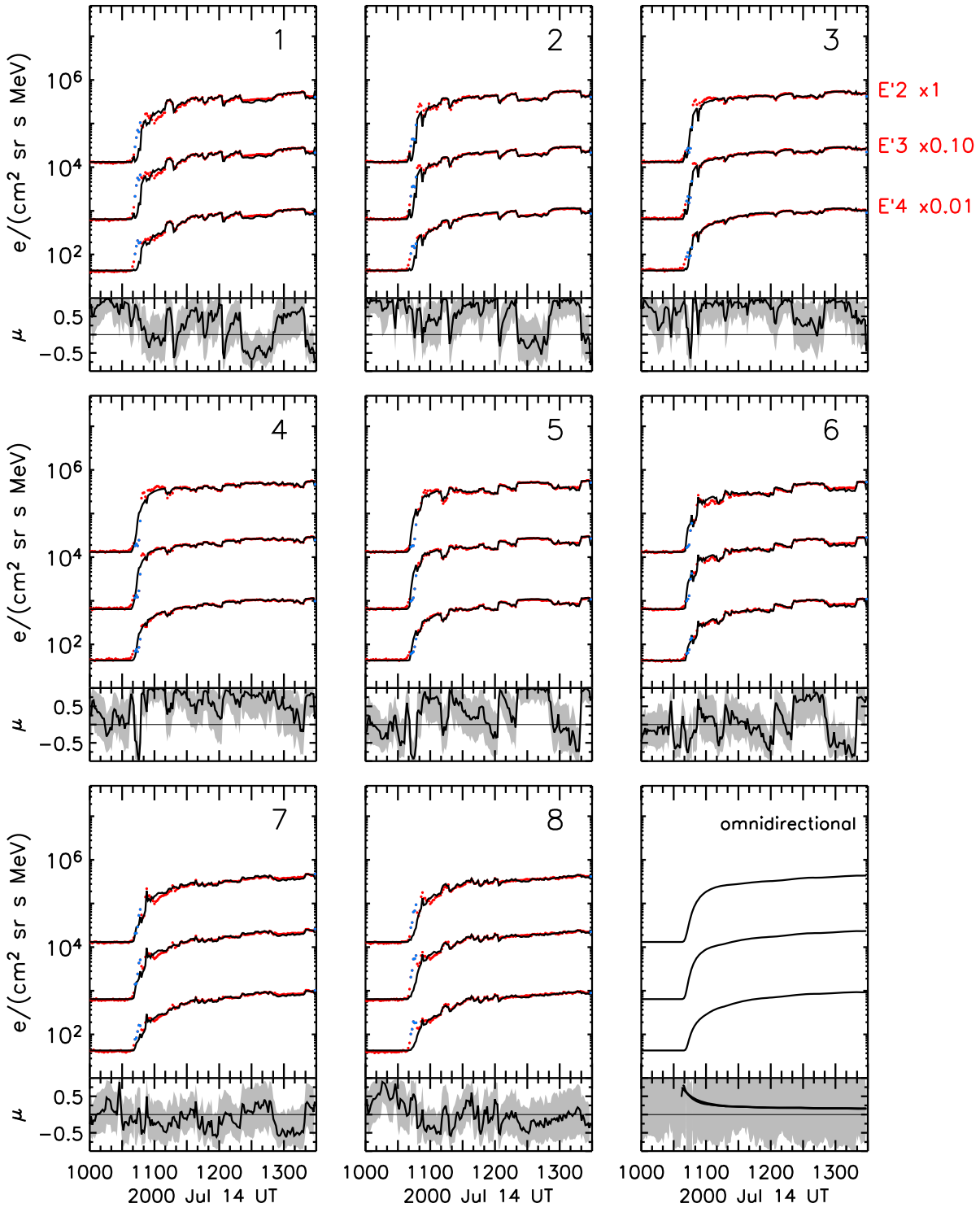

Figure 6.18: Jul00 event: Observational (red dots) and simulated (black line) sectored intensities. Blue dots indicate the data points excluded from the fit due to the reversal of IMF polarity. Same presentation as in Figure 5.4.

Table 6.4: Results of the fit

Scattering case	ζ {E'2, E'3, E'4}	λ_r (AU)
Isotropic scattering	{3, 2, 1} = 6	0.1
μ-dep with $\epsilon = 0.10$	{4, 3, 1} = 8	0.1
μ-dep with $\epsilon = 0.01$	{5, 3, 2} = 10	0.1

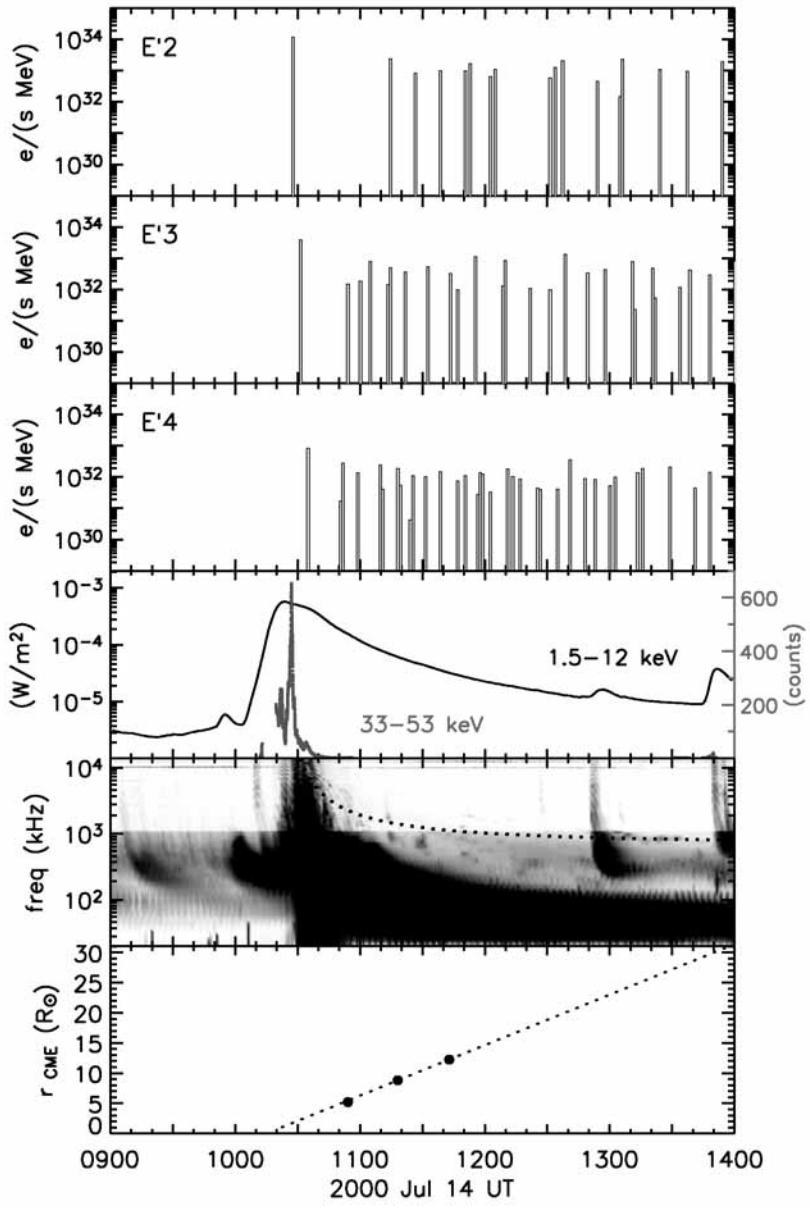

Figure 6.19: Jul00 event: Electron injection and associated electromagnetic emissions. Same presentation as in Figure 5.5.

By integrating the injection function over time for each energy channel, we find that the source spectrum can be best fit by a power-law with index $\gamma_s = 1.8$, as the total number of electrons in the E'2 channel is a bit lower than what the assumed spectral index ($\gamma_s = 2.1$) would demand.

The three lower panels of Figure 6.19 compare the timing of the electron injection with the associated electromagnetic emissions. We can see that the first prompt electron injection component in the E'2 energy channel is coincident with the hard X-ray burst observed by *Yohkoh*/HXR. In the three energy channels, the first injection component is coincident with the bright phase of the type III burst observed between 10:20 and 10:50 UT (Cane et al. 2002). In the early development of the event, radio sources spanned through the full visible range in longitude and large-scale loops were involved (Maia et al. 2001). Thus, it is plausible that the first injection component is associated with the flare, even though the AR location of the associated flare was somewhat far from the nominal footpoint.

The type II burst emission observed between 10:30 UT and 14:30 UT is consistent with being originated from a source located at the CME leading edge (dotted line in the fifth panel of Figure 6.19). This supports a scenario where the source of the time-extended injection component is, at least partly, provided by the CME-driven shock. In order to accept this scenario, we must assume that the source injecting NR electrons into the interplanetary medium moved from 2 $R_\odot$ to 30 $R_\odot$ during th period from 10:50 UT to 14:00 UT (see discussion in section 6.2.3 on the effect that the movement of the source has on the results of the modelization).

Bieber et al. (2001) proposed a different IMF configuration to explain the intensities observed during the Jul00 event; they assumed a magnetic compression beyond the Earth resulting from an earlier CME that passed eastward of Earth. To model the relativistic (~2 GeV) proton event, they assumed a barrier at 1.3 AU, with a reflection coefficient of 85%. The results of the simulation were found to be in good agreement with the density and anisotropy evolution of the relativistic proton observations. In addition, Bieber et al. (2001) attempted to simulate the 27–179 keV electron event observed by *Wind*/3DP and found that fitting the electrons was more complicated than fitting the protons, due to a possible second injection and to the temporary suppression of anisotropies from ~10:45 UT to 10:57 UT, very approximately the interval (from 10:44 UT to 10:50 UT) where there is a reversal of the IMF polarity that might explain the temporary suppression of anisotropies commented by these authors.

6.5 The 2001 April 15 event

6.5.1 Electromagnetic emissions

The 2001 April 15 (DOY 105) SEP event, also known as *Easter 2001* event, was associated with an X14.4 soft X-ray flare beginning at 13:19 UT and peaking 31 minutes later. Hard X-ray emission was observed starting at 13:44 UT (Bieber et al. 2004). Hα emission from a flare located at S20W85 began at 13:36 UT and peaked at 13:49 UT. Explosive motions in the low corona and locally close to the intense flare were observed in soft X-rays and EUV (Nitta et al. 2003).

A broad (167°) CME was first seen in LASCO C2 images over the west limb at 14:06 UT, at a projected central distance of ~4 $R_\odot$. The CME propagated at ~940 km s^{-1}. Maia et al. (2007) noted that although the CME seemed to decelerate from LASCO C3 field of view, this could be due to the loss of contrast produced by the 'snowstorm' of charged particles hitting the LASCO detectors. Cane et al. (2006) reported the passage of an interplanetary shock at *ACE* around 00:00 UT on April 18 (DOY 108) with a transit speed of 700 km s^{-1} (measured shock transit time from the Sun to 1 AU of ~60 h).

Maia et al. (2007) discussed the radio observations associated with this event in detail. The radio Sun was relatively calm during the early hours of 2001 April 15. The radio emission between 432 and 164 MHz displayed a major outburst slightly before 13:47 UT. After this major outburst, emissions at high frequencies showed a relatively smooth continuum, while the low ones showed a series of strong outbursts that lasted roughly 7 min. Maia et al. (2007) identified fast-moving radio loops moving outward with a velocity of about 1500 km s^{-1}, spatially coincident (at about the same position angle) with the white-light CME and showing similar kinematic behavior. Moreover, the radio and white-light loops had a similar morphology and expanded in a similar way. They differed, however, in angular extent; the radio loop was only the southern-most part of the CME (Maia et al. 2007). An occasional type II radio burst was reported by the *Wind*/WAVES experiment beginning around 14:05 UT and lasting 23 h.

6.5.2 In-situ energetic particles

The parent solar activity was accompanied by a large particle flux enhancement in interplanetary space. The SEP event extended to high energies, producing a ground level enhancement (GLE; Bieber et al. 2004).

Figure 6.20 shows the spin-averaged 62–312 keV electron intensities observed by the

LEFS60 telescope from April 15 (DOY 105) to April 19 (DOY 109). The first NR electrons were detected above the pre-event intensity background around 105/14:02 UT in the E'4 channel. The electron PADs observed immediately after the onset and during the rising phase of the event were broader than the instrument resolution, suggesting that incoming electrons had undergone considerable scattering (Maia et al. 2007). The maximum spin-averaged intensity was observed on 105/16:24 UT in the E'4 channel, on 105/16:24 UT in the E'3 channel and on 105/16:55 UT in the E'2 channel. We will study the NR electron event from 14:00 to 18:00 UT (gray area in Figure 6.20). For comparison, top panel of Figure 6.20 shows the DE30 electron intensities (thin line). The similarity of the profiles suggests that there is negligible ion contamination in the LEFS60 NR electron profiles during the period under study.

For completion, the top panel in Figure 6.20 also includes the 8-min spin-averaged proton intensities observed by the LEMS120 telescope and by the ERNE telescope (thin line) between 1 and 5 MeV approximately[13]. As can be seen, the proton event observed by *ACE* starts some minutes after the onset of the NR electron event and shows a prompt rise. The early onset suggests that P'7 and P'8 proton energy channels are contaminated by faster particles during the selected time period. The onset of the 1.90–4.75 MeV proton event observed by ERNE is registered ~90 min after the onset of the NR electron event, as expected.

The P'7 proton intensity rises from a pre-event level of 1×10^{1} to a level of 8×10^{2} particles $\mathrm{MeV^{-1}cm^{-2}sr^{-1}s^{-1}}$ in approximately 22 h; the maximum is observed on 106/14:00 UT. After the peak, the intensity profiles show a long decay phase. After 106/08:00 UT, NR electron intensities observed by the LEFS60 telescope mimic the proton intensity profiles and peak at the shock passage. DE30 electron intensities do not show such behavior, which suggests that the LEFS60 channels are contaminated by energetic protons after this time.

Using the *ACE*/SIS instrument, Cane et al. (2006) studied the event-averaged abundance of Fe relative to O, from 105/14:00 UT to 108/00:18 UT, and reported a ratio of Fe/O = 5.79 ± 0.15 relative to the average coronal value. Therefore, they concluded that this SEP event included flare-accelerated particles.

The four lower panels of Figure 6.20 show the solar wind velocity and the three components of the IMF in the RTN spacecraft coordinate system. The magnetic field components show large fluctuations, indicating a high level of solar wind turbulence (Dröge 2005). SWEPAM data indicate that during the NR electron event, *ACE* was embedded in a solar wind stream with a mean velocity 502 km $\mathrm{s^{-1}}$. The nominal footpoint of the field line connecting *ACE* to the Sun was at W48, far from the longitude of the flare site (W85). The

[13] In Figure 6.20, the ERNE measurements in the low energy channel (1.33–1.90 MeV) are multiplied by a factor 5, whereas measurements in the high energy channel (1.90–4.75 MeV) are multiplied by 0.5.

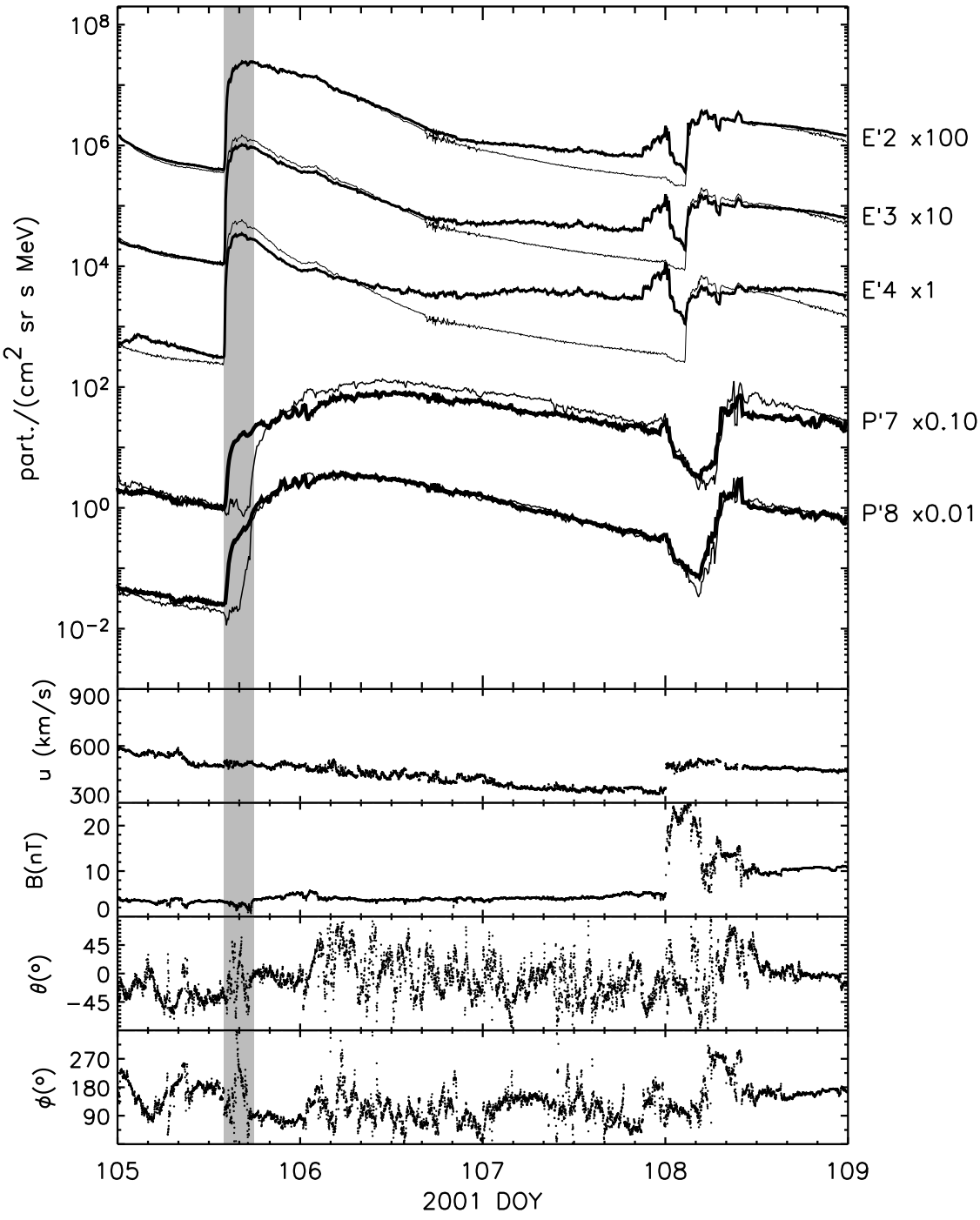

Figure 6.20: Apr01 event: Particle event, solar wind and magnetic field components in the RTN coordinate system. Same presentation as in Figure 5.1.

spectral index of the derived differential intensity spectrum is $\gamma = 1.8$, so we take $\gamma_s = 2.3$ as a first approximation of the spectral index of the electron source (see section 3.6).

6.5.3 Deconvolution of the NR electron event

Figure 6.21 shows the *ACE*/MAG magnetic field measurements in the spacecraft coordinate system, the range of μ-values scanned by the LEFS60 telescope and the μ-co of the telescope for the period under study. As can be seen, the IMF polarity remains negative during most of the period under study, with frequent reversals after 15:20 UT. The evolution of θ_B and ϕ_B during the change of polarity observed at ~15:30 UT seems to be associated with a rotation of the IMF. The μ-co of the telescope varies between 40% and 100%, with a mean coverage of μ-co ~87%. If we take into account only those time intervals with the modal polarity, the IMF direction is stable and the mean coverage of the telescope is of ~88%. As the telescope scans particles propagating antisunward along the field direction (see gray area in panel four) and μ-co $\geq$ 70%, sectored data provides a detailed description of the NR electron event.

We simulate this electron event following the procedure described in section 5.2.3 for the May00 event. In this case, we had to expand the tested range of λ_r values because the lowest value of ζ was obtained for $\lambda_r = 0.10$ AU; therefore, we have considered values of λ_r from 0.04 to 0.10 AU, with step intervals of 0.005 AU for $0.04 < \lambda_r < 0.08$ AU and of 0.02 AU for $0.08 < \lambda_r < 0.10$ AU. The lowest values of ζ obtained for each scattering case are listed in Table 6.5. Figure 6.22 shows the fit for the case with the lowest ζ; it corresponds to $\lambda_r = 0.06$ AU and μ-dependent scattering with $\epsilon = 0.01$. In this figure, the black curves show the modeled sectored intensities and the red dots the observational data. The blue dots mark the observational points excluded from the fit due to reversed IMF polarity. The optimum fit succeeds in reproducing most of the sectored intensity profiles. Differences between the observational and simulated sectored intensities from 15:20 to 16:20 UT are due to the change of polarity of the IMF and indicate that the injection history or the interplanetary transport conditions of NR electrons were slightly different in the flux tubes with opposite polarity.

The values of the solar electron injection derived from the best fit are shown in the three top panels of Figure 6.23. The injection profiles clearly show one prompt injection component starting around 13:50 UT in the three energy channels and lasting ~1 min. There is a second injection episode approximately from 14:30 UT to 15:30 UT and a few short dispersed injection episodes after 16:00 UT. The total number of injected NR electrons in the whole measurement range is $(13.6 \pm 0.6) \times 10^{34}$, as determined by the normalization of fitting. A large fraction (~56%) of the injection corresponds to the first component. The second component is weaker than the first one (it represents a ~30% of the whole injection); the last set

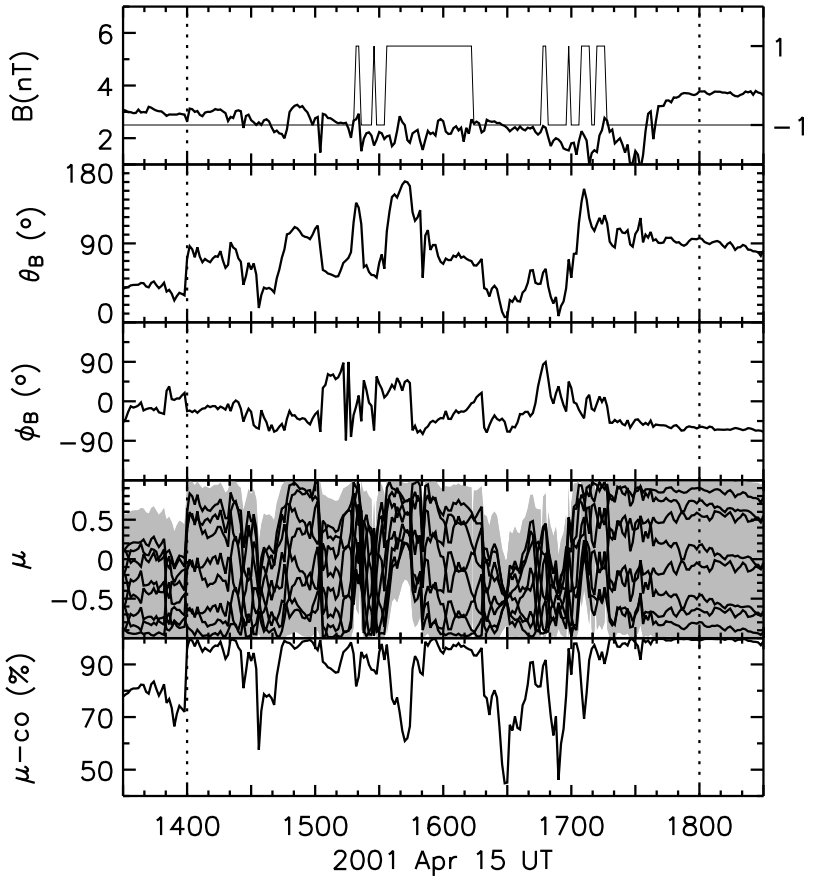

Figure 6.21: Apr01 event: IMF components in the spacecraft coordinate system; μ-range scanned by the LEFS60 telescope (gray area) and pitch-angle cosine of each sector; μ-co. Same presentation as in Figure 5.2.

of injection episodes represent ~14% of the total.

By integrating the injection function over time for each energy channel, we find that the source spectrum can be best fit by a power-law with index $\gamma_s = 2.1$, as the total number of electrons in the E'2 channel is a bit lower than what the assumed spectral index ($\gamma_s = 2.3$) would demand.

The lower three panels in Figure 6.23 compare the timing of the electron injection with the electromagnetic emissions observed at 1 AU. Comparing the times of the electron injection to the electromagnetic emissions, we find that the onset of the electron injection in E'2 is coincident with the hard X-rays burst. The first electron injection episode in E'3 and E'4 coincides with the major radio outburst reported at 13:50 UT in the 432–164 MHz frequency range (Maia et al. 2007) and also observed by *Wind*/WAVES (fifth panel in Figure 6.23). The first prompt injection component also seems to be related to the maximum in the soft X-ray flux profile, also at ~13:50 UT. The second injection is coincident with following radio

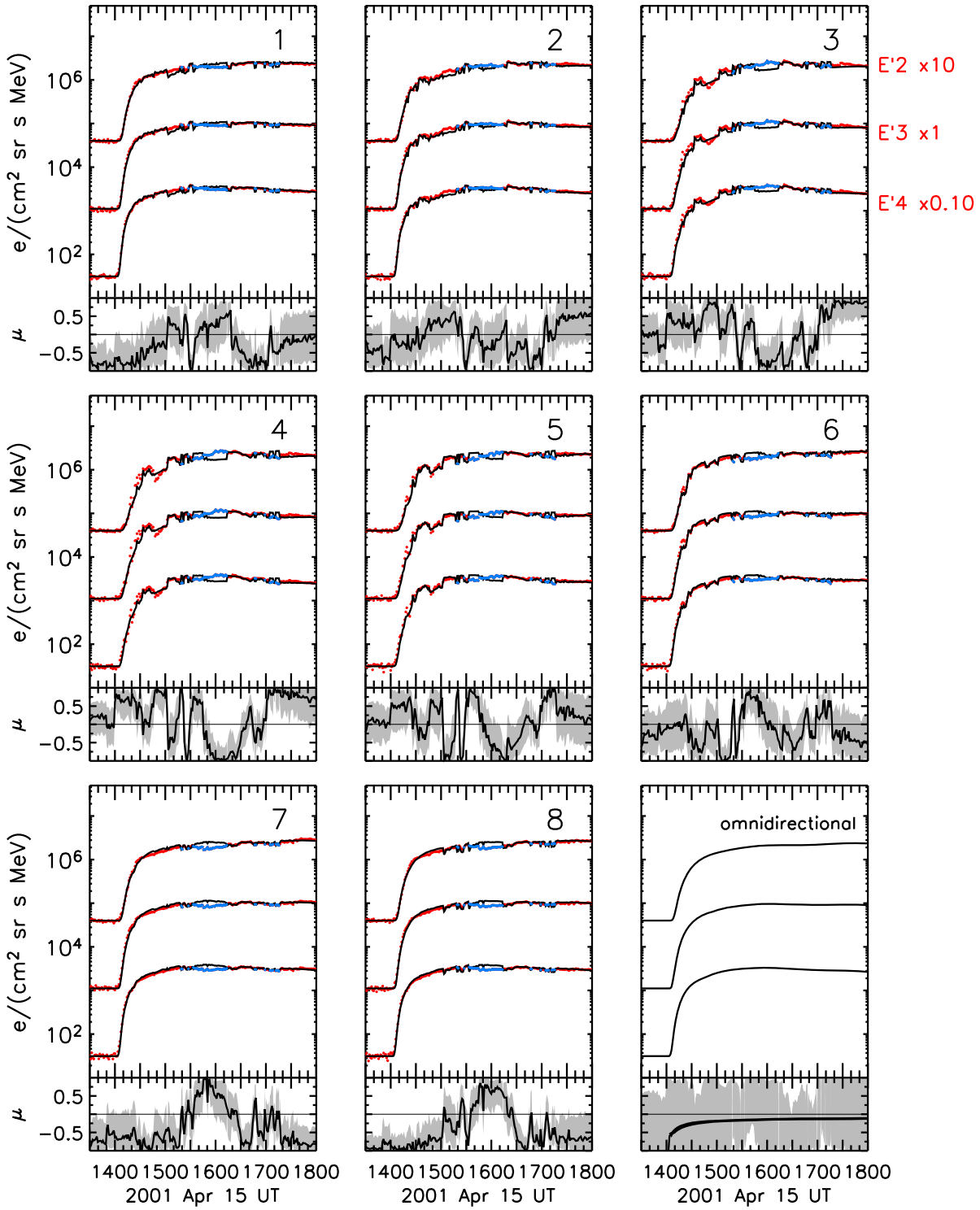

Figure 6.22: Apr01 event: Observational (red dots) and simulated (black line) sectored intensities. Blue dots indicate the data points excluded from the fit due to the reversal of polarity of the IMF. Same presentation as in Figure 5.4.

Table 6.5: Results of the fit

Scattering case	ζ {E'2, E'3, E'4}	λ_r (AU)
Isotropic scattering	{4, 4, 3} = 11	0.06
μ-dep with $\epsilon = 0.10$	{3, 3, 2} = 8	0.06
μ-dep with $\epsilon = 0.01$	{3, 2, 2} = 7	0.06

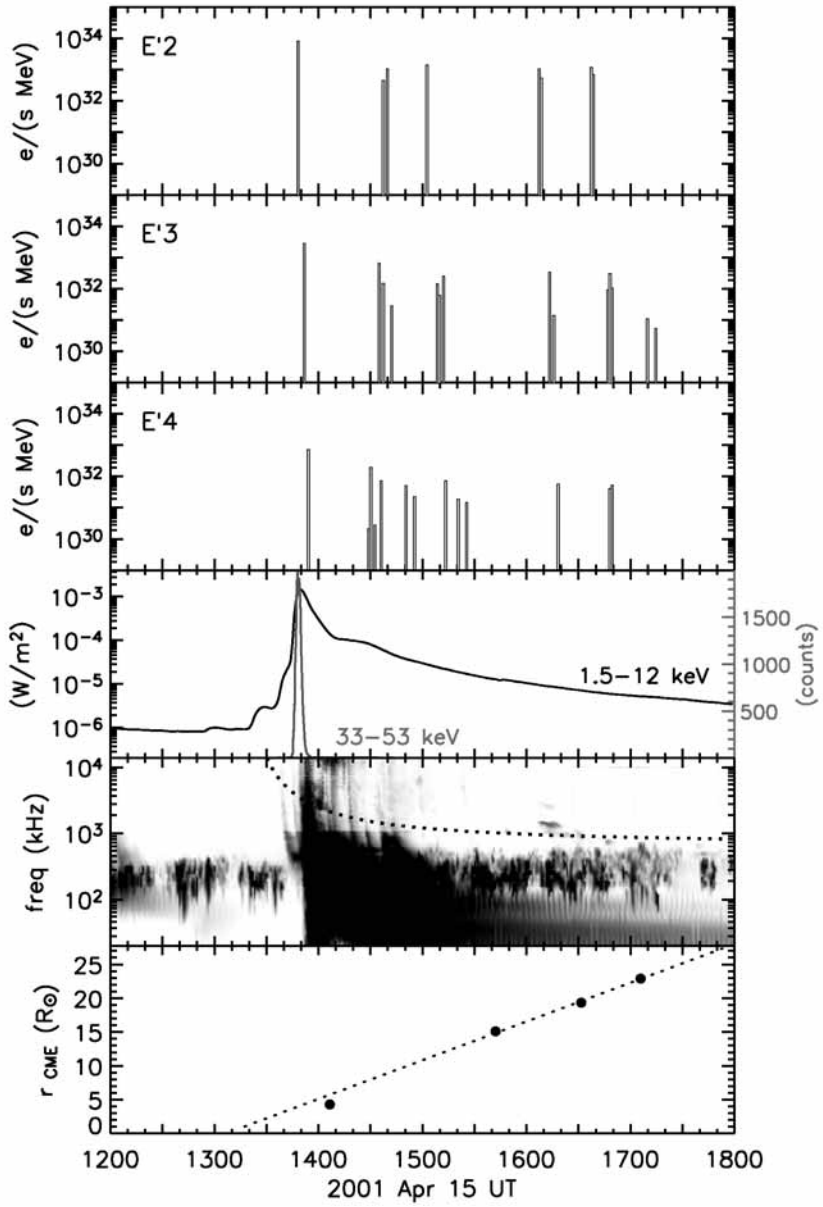

Figure 6.23: Apr01 event: Electron injection and associated electromagnetic emissions. Same presentation as in Figure 5.5.

emission, which is consistent with being originated from a source at a lower height than the CME leading edge (dotted line in the fifth panel of Figure 6.23). After 16:00 UT, the weak injection component seems to be related to a faint radio burst near 16:15 UT, which is consistent with being originated from close to the CME leading edge. Thus, the rising phase of the NR electron event observed by LEFS60 on 2001 April 15 seems to be primarily caused by flaring activity resulting from magnetic reconfiguring in the aftermath of the CME, as Maia et al. (2007) pointed out.

Tylka & Dietrich (2003) determined the release time of ions and electrons during this SEP event by using the c/v method. The ion and electron onset times at different energies were found to fall roughly on the same line, with an apparent propagation length of 1.7 AU and an estimated release time at the Sun of 13:44 UT (±1 min) – electromagnetic radiation emitted at that time would have been seen at the Earth at about 13:52 UT. Bieber et al. (2004) modeled the GLE (~2 GeV protons) taking into account propagation effects by solving the focused transport equation with a finite difference method. They deduced a proton injection profile with onset at 13:50 UT (±1 min) and peak at 13:56 UT, and $\lambda_r = 0.17$ AU.

Maia et al. (2007) modeled the 178–290 keV electron event observed by *ACE*, using a Monte Carlo transport model and deconvolving the spin-averaged intensities together with the averaged anisotropies. Maia et al. (2007) inferred a small λ_r between 0.04 and 0.05 AU, and a short (< 10 min) injection of electrons with the bulk of the particles being released around 13:50 UT. We obtained a slightly larger λ_r than Maia et al. (2007), and the same prompt injection but of shorter duration than 10 min. By studying a longer time period than Maia et al. (2007), we are able to infer two more injection episodes that seem to be consistent with electron injection from the CME leading edge.